Astronomy & Astrophysics manuscript no. babbage
February 1, 2008

Substructures in WINGS clusters ⋆

M. Ramella[1], A. Biviano[1], A. Pisani[2], J. Varela[3], D. Bettoni[3], W.J. Couch[4], M. D'Onofrio[5], A. Dressler[6], G. Fasano[3], P. Kjærgaard[7], M. Moles[8], E. Pignatelli[3], and B.M. Poggianti[3]

[1] INAF/Osservatorio Astronomico di Trieste, via G. B. Tiepolo 11, I-34131, Trieste, Italy
[2] Istituto di Istruzione Statale Classico Dante Alighieri, Scientifico Duca degli Abruzzi, Magistrale S. Slataper, viale XX settembre 11, I-34170 Gorizia, Italy
[3] INAF/Osservatorio Astronomico di Padova, vicolo Osservatorio 5, I-35122, Padova, Italy
[4] School of Physics, University of New South Wales, Sydney 2052, Australia
[5] Dipartimento di Astronomia, Università di Padova, vicolo Osservatorio 2, I-35122 Padova, Italy
[6] Observatories of the Carnegie Institution of Washington, Pasadena, CA 91101, USA
[7] Copenhagen University Observatory. The Niels Bohr Institute for Astronomy Physics and Geophysics, Juliane Maries Vej 30, 2100 Copenhagen, Denmark
[8] Instituto de Astrofísica de Andalucía (C.S.I.C.) Apartado 3004, 18080 Granada, Spain

Received / Accepted

ABSTRACT

Aims. We search for and characterize substructures in the projected distribution of galaxies observed in the wide field CCD images of the 77 nearby clusters of the WIde-field Nearby Galaxy-cluster Survey (WINGS). This sample is complete in X-ray flux in the redshift range $0.04 < z < 0.07$.
Methods. We search for substructures in WINGS clusters with DEDICA, an adaptive-kernel procedure. We test the procedure on Monte-Carlo simulations of the observed frames and determine the reliability for the detected structures.
Results. DEDICA identifies at least one reliable structure in the field of 55 clusters. 40 of these clusters have a total of 69 substructures at the same redshift of the cluster (redshift estimates of substructures are from color-magnitude diagrams). The fraction of clusters with subclusters (73%) is higher than in most studies. The presence of subclusters affects the relative luminosities of the brightest cluster galaxies (BCGs). Down to $L \sim 10^{11.2}\ L_{\odot}$, our observed differential distribution of subcluster luminosities is consistent with the theoretical prediction of the differential mass function of substructures in cosmological simulations.

Key words. Galaxies: clusters: general – Galaxies: kinematics and dynamics

1. Introduction

According to the current cosmological paradigm, large structures in the Universe form hierarchically. Clusters of galaxies are the largest structures that have grown through mergers of smaller units and have achieved near dynamical equilibrium. In the hierarchical scenario, clusters are a rather young population, and we should be able to observe their formation process even at rather low redshifts. A signature of such process is the presence of cluster substructures. A cluster is said to contain substructures (or subclusters) when its surface density is characterized by multiple, statistically significant peaks on scales larger than the typical galaxy size, with "surface density" being referred to the cluster galaxies, the intra-cluster (IC) gas or the dark matter (DM hereafter; Buote 2002).

Studying cluster substructure therefore allows us to investigate the process by which clusters form, constrain the cosmological model of structure formation, and ultimately test the hierarchical paradigm itself (e.g. Richstone et al. 1992; Mohr et al. 1995; Thomas et al. 1998). In addition, it also allows us to better understand the mechanisms affecting galaxy evolution in clusters, which can be accelerated by the perturbative effects of a cluster-subcluster collision and of the tidal field experienced by a group accreting onto a cluster (Bekki 1999; Dubinski 1999; Gnedin 1999). If clusters are to be used as cosmological tools, it is important to calibrate the effects substructures have on the estimate of their internal properties (e.g. Schindler & Müller 1993; Pinkney et al. 1996; Roettiger et al. 1998; Biviano et al. 2006; Lopes et al. 2006). Finally, detailed analyses of cluster substructures can be used to constrain the nature of DM (Markevitch et al. 2004; Clowe et al. 2006).

The analysis of cluster substructures can be performed using the projected phase-space distribution of cluster galaxies (e.g. Geller & Beers 1982), the surface-brightness distribution and temperature of the X-ray emitting IC gas (e.g. Briel et al. 1992), or the shear pattern in the background galaxy distribution induced by gravitational lensing, that directly samples substructure in the DM component (e.g. Abdelsalam et al. 1998). None of these tracers of cluster substructure (cluster galaxies, IC gas, background galaxies) can be considered optimal. The identification of substructures is in fact subject to different biases depending on the tracer used. In X-rays projection effects are less important than in the optical, but the identification of substructures is more subject to a z-dependent bias, arising from the point spread function of the X-ray telescope and detector (e.g. Böhringer & Schuecker 2002). Moreover, the different cluster components respond in a different way to a cluster-subcluster collision. The subcluster IC gas can be ram-pressure braked and stripped from the colliding subcluster and lags behind the subcluster galaxies and DM along the direction of collision (e.g.

Send offprint requests to: Massimo Ramella, ramella@oats.inaf.it
⋆ Figure 6 is only available in electronic form via http://www.edpsciences.org

Roettiger et al. 1997; Barrena et al. 2002; Clowe et al. 2006). Hence, it is equally useful to address cluster substructure analysis in the X-ray and in the optical.

Traditionally, the first detections of cluster substructures were obtained from the projected spatial distributions of galaxies (e.g. Shane & Wirtanen 1954; Abell et al. 1964), in combination, when possible, with the distribution of galaxy velocities (e.g. van den Bergh 1960, 1961; de Vaucouleurs 1961). Increasingly sophisticated techniques for the detection and characterization of cluster substructures have been developed over the years (see Moles et al. 1986; Perea et al. 1986a,b; Buote 2002; Girardi & Biviano 2002, and references therein). In many of these techniques substructures are identified as deviations from symmetry in the spatial and/or velocity distribution of galaxies and in the X-ray surface-brightness (e.g. West et al. 1988; Fitchett & Merritt 1988; Mohr et al. 1993; Schuecker et al. 2001). In other techniques substructures are identified as significant peaks in the surface density distribution of galaxies or in the X-ray surface brightness, either as residuals left after the subtraction of a smooth, regular model representation of the cluster (e.g. Neumann & Böhringer 1997; Ettori et al. 1998), or in a non-parametric way, e.g. by the technique of wavelets (e.g. Escalera et al. 1994; Slezak et al. 1994; Biviano et al. 1996) and by adaptive-kernel techniques (e.g. Kriessler & Beers 1997; Bardelli et al. 1998a, 2001).

The performances of several different methods have been evaluated both using numerical simulations (e.g. Mohr et al. 1995; Crone et al. 1996; Pinkney et al. 1996; Buote & Xu 1997; Cen 1997; Valdarnini et al. 1999; Knebe & Müller 2000; Biviano et al. 2006) and also by applying different methods to the same cluster data-sets and examine the result differences (e.g. Escalera et al. 1992, 1994; Mohr et al. 1995, 1996; Kriessler & Beers 1997; Fadda et al. 1998; Kolokotronis et al. 2001; Schuecker et al. 2001; Lopes et al. 2006). Generally speaking, the sensitivity of substructure detection increases with both increasing statistics (e.g. more galaxies or more X-ray photons) and increasing dimensionality of the test (e.g. using galaxy velocities in addition to their positions, or using X-ray temperature in addition to X-ray surface brightness).

Previous investigations have found very different fractions of clusters with substructure in nearby clusters, depending on the method and tracer used for substructure detection, on the cluster sample, and on the size of sampled cluster regions (e.g. Geller & Beers 1982; Dressler & Shectman 1988; Mohr et al. 1995; Girardi et al. 1997; Kriessler & Beers 1997; Jones & Forman 1999; Solanes et al. 1999; Kolokotronis et al. 2001; Schuecker et al. 2001; Flin & Krywult 2006; Lopes et al. 2006). Although the distribution of subcluster masses has not been determined observationally, it is known that subclusters of $\sim$ 10% the cluster mass are typical, while more massive subclusters are less frequent (Escalera et al. 1994; Girardi et al. 1997; Jones & Forman 1999). The situation is probably different for distant clusters which tend to show massive substructures more often than nearby clusters clearly suggesting hierarchical growth of clusters was more intense in the past (e.g. Gioia et al. 1999; van Dokkum et al. 2000; Haines et al. 2001; Maughan et al. 2003; Huo et al. 2004; Rosati et al. 2004; Demarco et al. 2005; Jeltema et al. 2005).

Additional evidence for the hierarchical formation of clusters is provided by the analysis of brightest cluster galaxies (BCGs hereafter) in substructured clusters. BCGs usually sit at the bottom of the potential well of their host cluster (e.g. Adami et al. 1998b). When a BCG is found to be significantly displaced from its cluster dynamical center, the cluster displays evidence of substructure (e.g. Beers et al. 1991; Ferrari et al. 2006). From the correlation between cluster and BCG luminosities, Lin & Mohr (2004) conclude that BCGs grow by merging as their host clusters grow hierarchically. The related evolution of BCGs and their host clusters is also suggested by the alignement of the main cluster and BCG axes (e.g. Binggeli 1982; Durret et al. 1998). Both the BCG and the cluster axes are aligned with the surrounding large scale structure distribution, where infalling groups come from. These infalling groups are finally identified as substructures once they enter the cluster environment (Durret et al. 1998; Arnaud et al. 2000; West & Blakeslee 2000; Ferrari et al. 2003; Plionis et al. 2003; Adami et al. 2005). Hence, substructure studies really provide direct evidence for the hierarchical formation of clusters.

Concerning the impact of subclustering on global cluster properties, it has been found that subclustering leads to overestimating cluster velocity dispersions and virial masses (e.g. Perea et al. 1990; Bird 1995; Maurogordato et al. 2000), but not in the general case of small substructures (Escalera et al. 1994; Girardi et al. 1997; Xu et al. 2000). During the collision of a subcluster with the main cluster, both the X-ray emitting gas distribution and its temperature have been found to be significantly affected (e.g. Markevitch & Vikhlinin 2001; Clowe et al. 2006). As a consequence, it has been argued that substructure can explain at least part of the scatter in the scaling relations of optical-to-X-ray cluster properties (e.g. Fitchett 1988; Girardi et al. 1996; Barrena et al. 2002; Lopes et al. 2006).

As far as the internal properties of cluster galaxies are concerned, there is observational evidence that a higher fraction of cluster galaxies with spectral features characteristic of recent or ongoing starburst episodes is located in substructures or in the regions of cluster-subcluster interactions (Caldwell et al. 1993; Abraham et al. 1996; Biviano et al. 1997; Caldwell & Rose 1997; Bardelli et al. 1998b; Moss & Whittle 2000; Miller et al. 2004; Poggianti et al. 2004; Miller 2005; Giacintucci et al. 2006).

In this paper we search for and characterize substructures in the sample of 77 nearby clusters of the WIde-field Nearby Galaxy-cluster Survey (WINGS hereafter, Fasano et al. 2006). This sample is an almost complete sample in X-ray flux in the redshift range $0.04 < z < 0.07$. We detect substructures from the spatial, projected distribution of galaxies in the cluster fields, using the adaptive-kernel based DEDICA algorithm (Pisani 1993, 1996). In Sect. 2 we describe our data-set; in Sect. 3 we describe the procedure of substructure identification; in Sect. 4 we use Monte Carlo simulations in order to tweak our procedure; in Sect. 5 we describe the identification of substructures in our data-set; in Sect. 6 the catalog of identified substructures is provided. In Sect. 7 we investigate the properties of the identified substructures, and in Sect. 8 we consider the relation between the BCGs and the substructures. We provide a summary of our work in Sect. 9.

2. The Data

WINGS is an all-sky, photometric (multi-band) and spectroscopic survey, whose global goal is the systematic study of the local cosmic variance of the cluster population and of the properties of cluster galaxies as a function of cluster properties and local environment.

The WINGS sample consists of 77 clusters selected from three X-ray flux limited samples compiled from ROSAT All-Sky Survey data, with constraints just on the redshift ($0.04 < z < 0.07$) and distance from the galactic plane ($|b| \geq 20$ deg). The core

of the project consists of wide-field optical imaging of the selected clusters in the *B* and *V* bands. The imaging data were collected using the WFC@INT (La Palma) and the WFI@MPG (La Silla) in the northern and southern hemispheres, respectively.

The observation strategy of the survey favors the uniformity of photometric depth inside the different CCDs, rather than complete coverage of the fields that would require dithering. Thus, the gaps in the WINGS optical imaging correspond to the physical gaps between the different CCDs of the mosaics.

During the data reduction process, we give particular care to sky subtraction (also in presence of crowded fields including big halo galaxies and/or very bright stars), image cleaning (spikes and bad pixels) and star/galaxy classification (obtained with both automatic and interactive tools).

According to Fasano et al. (2006) and Varela et al. (2007), the overall quality of the data reported in the WINGS photometric catalogs can be summarized as follows: (i) the astrometric errors for extended objects have *r.m.s.* ∼0.2 arcsec; (ii) the average limiting magnitude is ∼24.0, ranging from 23.0 to 25.0; (iii) the completeness of the catalogs is achieved (on average) up to V ∼22.0; (iv) the total (systematic plus random) photometric *r.m.s.* errors, derived from both internal and external comparisons, vary from ∼0.02 mag, for bright objects, up to ∼0.2 mag, for objects close to the detection limit.

3. The DEDICA Procedure

We base our search for substructures in WINGS clusters on the DEDICA procedure (Pisani 1993, 1996). This procedure has the following advantages:

1. DEDICA gives a total description of the clustering pattern, in particular the membership probability and significance of structures besides geometrical properties;
2. DEDICA is scale invariant;
3. DEDICA does not assume any property of the clusters, i.e. it is completely non-parametric. In particular it does not require particularly rich samples to run effectively.

The basic nature and properties of DEDICA are described in Pisani (1993, 1996, and references therein). Here we summarize the main structure of the algorithm and how we apply it to our data sample. The core structure of DEDICA is based on the assumption that a structure (or a "cluster" in the algorithm jargon) corresponds to a local maximum in the density of galaxies.

We proceed as follows. First we need to estimate the probability density function $\Psi(\mathbf{r}_i)$ (with $i = 1, \ldots N$) associated with the set of N galaxies with coordinates $\mathbf{r}_i$. Second, we need to find the local maxima in our estimate of $\Psi(\mathbf{r}_i)$ in order to identify clusters and also to evaluate their significance relatively to the noise. Third and finally, we need to estimate the probability that a galaxy is a member of the identified clusters.

3.1. The probability density

DEDICA is a non-parametric method in the sense that it does not require any assumption on the probability density function that it is aimed to estimate. The only assumptions are that $\Psi(\mathbf{r}_i)$ must be continuous and at least twice differentiable.

The function $f(\mathbf{r}_i)$ is an estimate of $\Psi(\mathbf{r}_i)$ and it is built by using an adaptive kernel method given by:

$$f_{ka}(\mathbf{r}) = \frac{1}{N}\sum_{i=1}^{N} K(\mathbf{r}_i, \sigma_i; \mathbf{r}) \tag{1}$$

where we use the two dimensional Gaussian kernel $K(\mathbf{r}_i, \sigma_i; \mathbf{r})$ centered in $\mathbf{r}_i$ with size σ_i.

The most valuable feature of DEDICA is the procedure to select the values of kernel widths σ_i. It is possible to show that the optimal choice for σ_i, i.e. with asymptotically minimum variance and null bias, is obtained by minimizing the distance between our estimate $f(\mathbf{r}_i)$ and $\Psi(\mathbf{r}_i)$. This distance can be evaluated by a particular function called the integrated square error $ISE(f)$ given by:

$$ISE(f) = \int_{\Re} [\Psi(\mathbf{r}) - f(\mathbf{r})]^2 d\mathbf{r} \tag{2}$$

.

Once the minimum $ISE(f)$ is reached we have obtained the DEDICA estimate of the density as in Eq.1.

3.2. Cluster Identification

The second step of DEDICA consists in the identification of the local maxima in $f_{ka}(\mathbf{r})$. The positions of the peaks in the density function $f_{ka}(\mathbf{r})$ are found as the solutions of the iterative equation:

$$\mathbf{r}_{m+1} = \mathbf{r}_m + a \cdot \frac{\nabla f_{ka}(\mathbf{r}_m)}{f_{ka}(\mathbf{r}_m)} \tag{3}$$

where a is a scale factor set according to optimal convergence requirements. The limit $\mathbf{R}$ of the sequence $\mathbf{r}_m$ defined in Eq.3 depends on the starting position $\mathbf{r}_{m=1}$.

$$\lim_{m\to+\infty} \mathbf{r}_m = \mathbf{R}(\mathbf{r}_{m=1}) \tag{4}$$

We run the sequence in Eq.3 at each data position $\mathbf{r}_i$. We label each data point with the limit $\mathbf{R}_i = \mathbf{R}(\mathbf{r}_{m=1} = \mathbf{r}_i)$. These limits $\mathbf{R}_i$ are the position of the peak to which the $i-th$ galaxy belong. In the case that all the galaxies are members of a unique cluster, all the labels $\mathbf{R}_i$ are the same. At the other extreme each galaxy is a one-member cluster and all $\mathbf{R}_i$ have different values. All the members of a given cluster belong to the same peak in $f_{ka}(\mathbf{r})$ and have the same $\mathbf{R}_i$. We identify cluster members by listing galaxies having the same values of $\mathbf{R}$. We end up with ν different clusters each with n_μ ($\mu = 1, \ldots, \nu$) members.

In order to maintain a coherent notation, we identify with the label $\mu = 0$ the n_0 isolated galaxies considered a system of background galaxies. We have: $n_0 = N - \sum_{\mu=1}^{\nu} n_\mu$.

3.3. Cluster Significance and of Membership Probability

The statistical significance S_μ ($\mu = 1, \ldots, \nu$) of each cluster is based on the assumption that the presence of the $\mu - th$ cluster causes an increase in the local probability density as well as in the sample likelihood $L_N = \Pi_i[f_{ka}(\mathbf{r}_i)]$ relatively to the value L_μ that one would have if the members of the $\mu - th$ cluster were all isolated, i.e. belonging to the background.

A large value in the ratio L_N/L_μ characterizes the most important clusters. According to Materne (1979) it is possible to estimate the significance of each cluster by using the likelihood ratio test. In other words $2\ln(L_N/L_\mu)$ is distributed as a χ^2 variable with $\nu - 1$ degrees of freedom. Therefore, once we compute the value of χ^2 for each cluster (χ^2_S), we can also compute the significance S_μ of the cluster.

Here we assume that the contribution to the global density field $f_{ka}(\mathbf{r}_i)$ of the $\mu - th$ cluster is $F_\mu(\mathbf{r}_i)$. The ratio between the value of $F_\mu(\mathbf{r}_i)$ and the total local density $f_{ka}(\mathbf{r}_i)$ can be used to estimate the membership probability of each galaxy relatively to

the identified clusters. This criterion also allows us to estimate the probability that a galaxy is isolated.

At the end of the DEDICA procedure we are left with a) a catalog of galaxies each with information on position, membership, local density and size of the Gaussian kernel, b) a catalog of structures with information on position, richness, the χ^2_S parameter, and peak density. For each cluster we also compute from the coordinate variance matrix the cluster major axis, ellipticity and position angle.

4. Tweaking the Algorithm with Simulations

In this section we describe our analysis of the performance of DEDICA and the guidelines we obtain for the interpretation of the clustering analysis of our observations.

We build simulated fields containing a cluster with and without subclusters. The simulated fields have the same geometry of the WFC field and are populated with the typical number of objects we will analyze. For simplicity we consider only WFC fields. Because DEDICA is scale-free, a different sampling of the same field of view has no consequence on our analysis.

In the next section we limit our analysis to $M_{V,lim} \leq -16$. At the median redshift of the WINGS cluster, $z \simeq 0.05$, this absolute magnitude limit corresponds to an apparent magnitude $V_{lim} \simeq 21$. Within this magnitude limit the representative number of galaxies in our frames is N_{tot}= 900.

We then consider N_{tot}= N_{mem}+ N_{bkg}, with $N_{mem}$the number of cluster members and $N_{bkg}$the number of field – or background – galaxies. We set N_{bkg}= 670, close to the average number of background galaxies we expect in our frame based on typical observed fields counts, e.g. Berta et al. (2006) or Arnouts et al. (1997). With this choice, we have N_{mem}= 230.

We distribute uniformly at random N_{bkg}objects. We distribute at random the remaining N_{mem}= 230 objects in one or more overdensities depending on the test we perform. We populate overdensities according to a King profile (King 1962) with a core radius R_{core} = 90 kpc, representative of our clusters. We then scale R_{core} with the number of members of the substructure, N_S. We use

$$R_{core} = 250 \sqrt{\frac{N_S}{N_C + N_S}}$$

where N_C is the number of objects in the cluster with N_{mem}= N_S + N_C. This scaling of R_{core} with cluster richness is from Adami et al. (1998a) assuming direct proportionality between cluster richness and luminosity (e.g. Popesso et al. 2006).

As far as the relative richnesses of the cluster and subcluster are concerned, we consider the following richness ratios r_{cs} = N_C/N_S = 1, 2, 4, 8. With these richness ratios, the number of objects in the cluster are N_C = 115, 153, 184, 204, and those in subclusters are N_S = 115, 77, 46, 26 respectively.

In a first set of simulated fields we place the substructure at 2731 pixels (15 arcmin) from the main cluster so that they do not overlap. In a second set of simulations, we place main cluster and substructure at shorter distances, 683 and 1366 pixels, in order to investigate the ability of DEDICA to resolve structures. At each of these shorter distances we build simulations with both r_{cs}= 1 and 2.

For each richness ratio and/or distance between cluster and subcluster we produce 16 simulations with different realizations of the random positions of the data points representing galaxies.

In order to minimize the effect of the borders on the detection of structures we add to the simulation a “frame” of 1000 pixel.

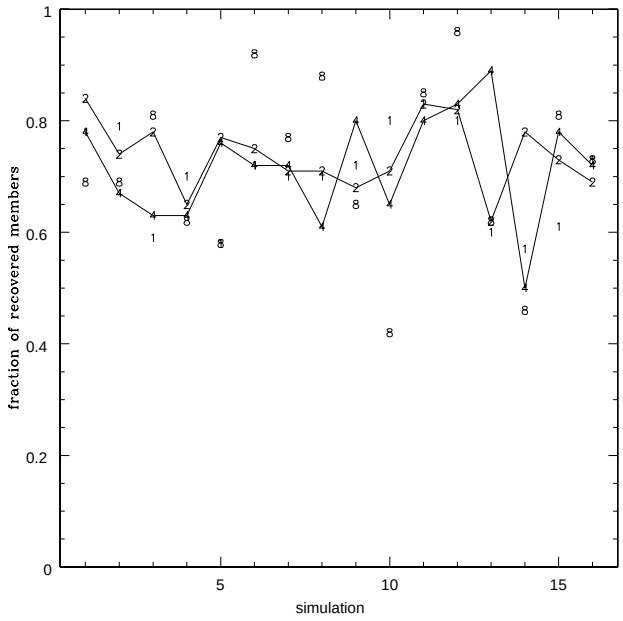

Fig. 1. Fraction of recovered members of each substructure for different r_{cs}. The solid line connects substructures with r_{cs} = 2 and 4

We fill this frame with a grid of data points at the same density as the average density of the field.

The first result we obtain from the runs of DEDICA on the simulations with varying richness ratio is the positive rate at which we detect real structures. We find that we always recover both cluster and substructure even when the substructure only contains N_S = 1/8 N_C objects, i.e. 26 objects (on top of the uniform background). In other words, if there is a real structure DEDICA finds it.

We also check how many original members the procedure assigns to structures it recovers. The results are summarized in Fig. 1. In the diagram, the fraction of recovered members of each substructure is represented by the values of its r_{cs}. The solid line connects substructures with r_{cs} = 2 and 4.

From Fig. 1 it is clear that our procedure recovers a large fraction of members, almost irrespective of the richness of the original structure. It is also interesting to note that the fluctuations identified as substructures are located very close to the center of the corresponding simulated substructures. In almost all cases the distance between original and detected substructure is significantly shorter than the mean inter-particle distance.

The second important result we obtain from the simulations is the false positive rate, i.e. the fraction of noise fluctuations that are as significant as the fluctuations corresponding to real structures.

First of all we need to define an operative measure of the reliability of the detected structures. In fact DEDICA provides a default value S_μ ($\mu = 1, \ldots, \nu$) of the significance (see Sect. 3.3). However, S_μ has a relatively small dynamical range, in particular for highly significant clusters.

Density or richness both allow a reasonable ”ranking” of structures. However, both large low-density noise fluctuations (often built up from more than one noise fluctuation) and very high density fluctuations produced by few very close data points could be mistakenly ranked as highly significant structures according to, respectively, richness and density criteria.

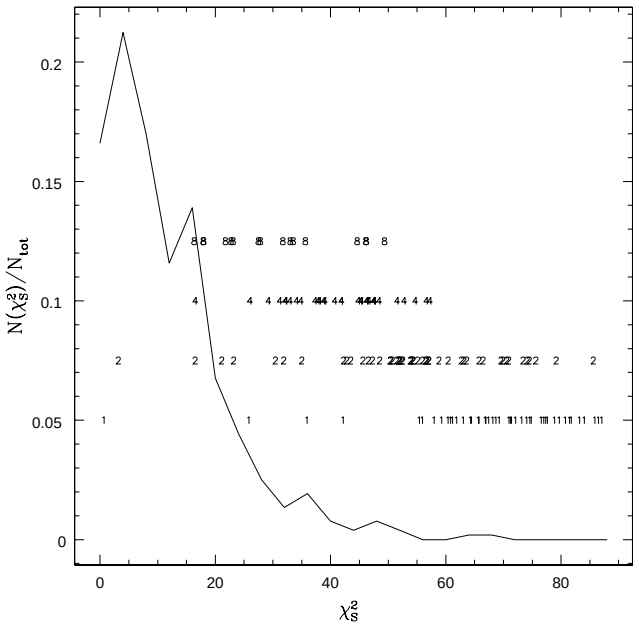

Fig. 2. χ^2_S of simulated noise fluctuations (solid line). Labels are the r_{cs} of simulated structures at the abscissa corresponding to their χ^2_S and at arbitrary ordinates.

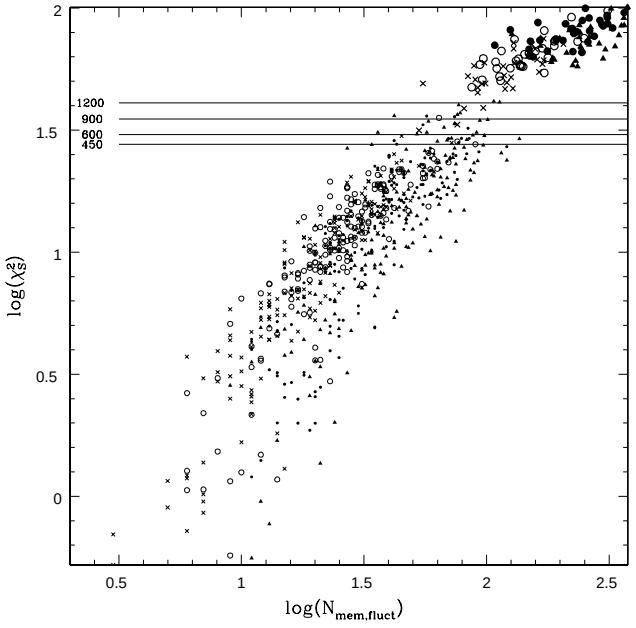

Fig. 3. Small symbols correspond to χ^2_S as a function of the number of members of noise fluctuations. Crosses, circles, dots and triangles are χ^2_S for the noise fluctuations of the simulations with N_{tot}= 450, 600, 900, and 1200 respectively. Large symbols are χ^2_S of simulated clusters and subclusters with r_{cs}= 1. Horizontal lines mark the levels of $\chi^2_{S,threshold}$.

We therefore prefer to use the parameter χ^2_S which stands at the base of the estimate of S_μ and which is naturally provided by DEDICA. The main characteristic of χ^2_S is that it depends *both* on the density of a cluster relative to the background and on its richness. Using χ^2_S we classify correctly significantly more structures than with either density or richness alone.

In Fig. 2 we plot the distribution of χ^2_S of noise fluctuations (solid line). In the same plot we also mark the r_{cs} of real structures as detected by our procedure. We use labels indicating r_{cs} and place them at the abscissa corresponding to their χ^2_S and at arbitrary ordinates.

Fig. 2 shows that the structures detected with r_{cs}= 1, 2 are always distinguishable from noise fluctuations. Substructures with r_{cs}= 4 or higher, although correctly detected, have χ^2_S values that are close to or lower than the level of noise.

With the second set of simulations, we test the minimum distance at which cluster and subcluster can still be identified as separate entities. We place cluster and substructure (r_{cs}= 1, 2) at distances d_{cs} = 683 and 1366 pixel. These distances are 1/4 and 1/2 respectively of the distance between cluster and substructure in the first set of simulations. Again we produce 16 simulations for each of the 4 cases.

We find that at d_{cs} = 1366 pixel cluster and substructure are always correctly identified. At the shorter distance d_{cs} = 683 pixel, DEDICA merges cluster and substructure in 1 out of 16 cases for r_{cs}= 1 and in 8 out of 16 cases for r_{cs}= 2. With our density profile, d_{cs} = 683 pixel corresponds to $d_{cs} \simeq R_c + R_s$ with R_c, R_s the radii of the main cluster and of the subcluster respectively.

In order to verify the results we obtain for 900 data points we produce more simulations with N_{tot}= 450, 600 and 1200. In all these simulations R_C and R_S are the same as in the set with N_{tot}= 900. We vary N_{bkg} and N_{mem} so that N_{mem}/ N_{bkg} is the same as in the case N_{tot}= 900.

These simulations confirm the results we obtain in the case N_{tot}= 900, and allow us to set a detection threshold, $\chi^2_{S,threshold}(N_{tot})$, for significant fluctuations in the analysis of real clusters.

We summarize the behavior of the noise fluctuations in our simulations in Fig. 3. In this figure, the small symbols correspond to χ^2_S as a function of the number of members of noise fluctuations. In particular, crosses, circles, dots and triangles are χ^2_S for the noise fluctuations of the simulations with N_{tot}= 450, 600, 900, and 1200 respectively.

The larger symbols are the χ^2_S of the fluctuations corresponding to simulated clusters and subclusters of equal richness (r_{cs}= 1).

The 4 horizontal lines mark the level of $\chi^2_{S,threshold}$, i.e. the average χ^2_S of the 3 most significant noise fluctuations in each of the 4 groups of simulations with N_{tot}= 450, 600, 900, and 1200.

The expected increase of $\chi^2_{S,threshold}$ with N_{tot} is evident.

We note that the only significant difference with these findings we obtain from the simulations with r_{cs}= 2 is that χ^2_S of simulated clusters and subclusters is closer to $\chi^2_{S,threshold}$ (but still higher).

We fit $\chi^2_{S,threshold}$ with N_{tot} and obtain

$$\log(\chi^2_{S,threshold}) = 1/2.55\ \log(N_{tot}) + 0.394 \quad (5)$$

in good agreement with the expected behavior of the poissonian fluctuations.

As a final test we verify that infra-chip gaps do not have a dramatic impact on the detection of structures in the cases r_{cs}= 1 and 2. We place a 50 pixel wide gap where it has the maximum impact, i.e. where the kernel size is shortest. Even if the infra-

chip gap cuts through the center of the structures, DEDICA is able to identify these structures correctly.

We summarize here the main results of our tests on simulated clusters with substructures:

- DEDICA successfully detects even the poorest structures above a uniform poissonian noise background.
- DEDICA recovers a large fraction (typically > 3/4) of the real members of a substructure, almost irrespective of the richness of the structure.
- DEDICA is able to distinguish between noise fluctuations and true structures only if these structures are rich enough. In the case of our simulations, structures have to be richer than 1/4th of the main structure.
- DEDICA is able to separate neighboring structures provided they do not overlap.
- infra-chip gaps do not threaten the detection of structures that are rich enough to be reliably detected.
- the χ^2_S threshold we use to identify significant structures is a function of the total number of points and can be scaled within the whole range of numbers of galaxies observed within our fields.

In the next section we apply these results to the real WINGS clusters.

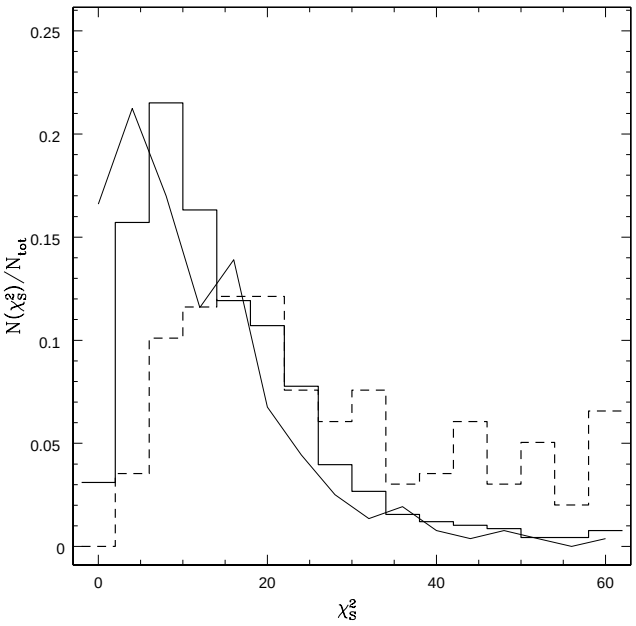

Fig. 4. χ^2_S distributions for border (thick solid histogram) and central (thick dashed histogram) observed fluctuations. The thin solid line is the normalized distribution of χ^2_S of the noise fluctuations in our simulations

5. Substructure detection in WINGS clusters

We apply our clustering procedure to the 77 clusters of the WINGS sample. The photometric catalog of each cluster is deep, reaching a completeness magnitude $V_{complete} \leq 22$. The number of galaxies is correspondingly large, from $N_{gal} \simeq 3,000$ to $N_{gal} \simeq 10,000$.

The large number of bright background galaxies (faint apparent magnitudes) dilutes the clustering signal of local WINGS clusters. We perform test runs of the procedure on several clusters with magnitude cuts brighter than $V_{complete}$. Based on these tests, we decide to cut galaxy catalogs to the absolute magnitude threshold $M_V = -16.0$. With this choice a) we maximize the signal-to-noise ratio of the detected subclusters and b) we still have enough galaxies for a stable identification of the system. At the median redshift of WINGS clusters, $z \simeq 0.0535$, our absolute magnitude cut corresponds to an apparent magnitude $V \simeq 21.2$.

This apparent magnitude also approximately corresponds to the magnitude where the contrast of our typical cluster relative to the field is maximum (this estimate is based on the average cluster luminosity function of (Yagi et al. 2002; De Propris et al. 2003) and on the galaxy counts of (Berta et al. 2006)).

The number of galaxies that are brighter than the threshold $M_V = -16.0$ is in the range $600 < N_{tot} < 1200$ for a large fraction of clusters observed with either WFC@INT or with WFI@ESO2.2.

In order to proceed with the identification of significant structures within WINGS clusters, we need to verify that our simulations are sufficiently representative of the real cases. In practice we need to compare the observed distributions of χ^2_S values of noise fluctuations with the corresponding simulated distributions. In the observations it is impossible to identify individual fluctuations as noise. In order to have an idea of the distributions of χ^2_S of noise fluctuations we consider that our fields are centered on real clusters. As a consequence, on average, fluctuations in the center of the frames are more likely to correspond to real systems than those at the borders.

We therefore consider separately the fluctuations within the central regions of the frames and all other fluctuations (borders). We define the central regions as the central 10% of WFC and WFI areas. We plot in Fig. 4 the two distributions. The thick solid histogram is for the border and the thick dashed histogram for the center of the frames. The difference between "noise" and "signal" is clear. In the same figure we also plot the normalized distribution of χ^2_S of the noise fluctuations in our simulations (thin solid line). The distributions of χ^2_S of the observed and simulated fluctuations are in reasonable agreement considering a) the simple model used for the simulations and that b) in the observations we can not exclude real low-χ^2_S structures among noise fluctuations. We conclude that for our clusters we can adopt the same reliability threshold $\chi^2_{S,threshold}$ we determine from our simulations (Eq. 5).

6. The Catalog of Substructures

We detect at least one significant structure in 55 (71%) clusters. We find that 12 clusters (16%) have no structure above the threshold (undetected). In the case of another 10 (13%) clusters we find significant structures only at the border of the field of view. In absence of a detection in the center of the frame, we consider these border structures unrelated to the target cluster. We also verify that in the Color-Magnitude Diagram (CMD) these border structures are redder than expected given the redshift of the target cluster. We consider also these 10 clusters undetected.

Here we list the 22 undetected clusters: A0133, A0548b, A0780, A1644, A1668, A1983, A2271, A2382, A2589, A2626, A2717, A3164, A3395, A3490, A3497, A3528a, A3556, A3560, A3809, A4059, RX1022, Z1261.

We note that undetected clusters are real physical systems according to their x-ray selection. From an operative point of view, the fact that these clusters are not detected by DEDICA is the

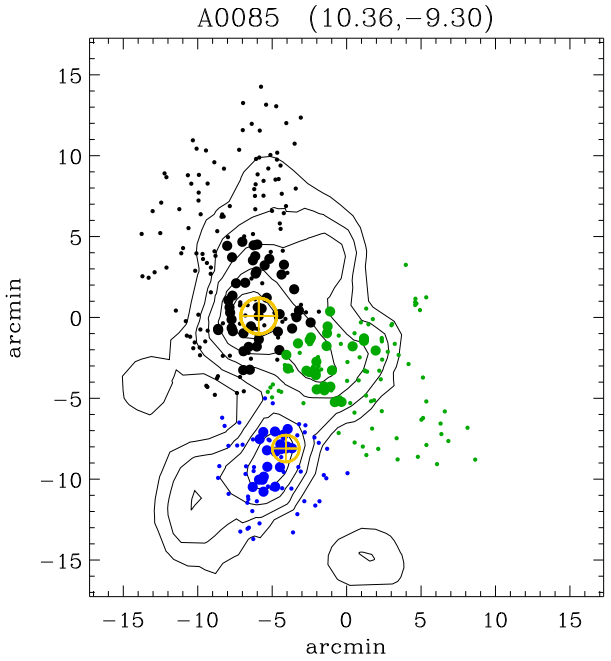

Fig. 5. Isodensity contours (logarithmically spaced) of the Abell 85 field. The title lists the coordinates of the center. The orientation is East to the left, North to the top. Galaxies belonging to the systems detected by DEDICA are shown as dots of different colors. Black, light green, blue, red, magenta, dark green are for the main system and the subsequent substructures ordered as in Table A.1. Large symbols are for galaxies with $M_V \leq -17.0$ that lie where local densities are higher than the median local density of the structure the galaxy belongs to. Open symbols mark the positions of the first- and second-ranked cluster galaxies, BCG1 and BCG2 respectively. Similar plots for the 55 analysed clusters are available in the electronic version of this Journal.

result of the division into too many structures of the total available clustering signal in the field (or of a too large fraction of the clustering signal going into border structures). Several physical situations could be at the origin of missed detections. One possibility is an excess of physical substructures of comparable richness. Another possibility is that these clusters are embedded in regions of the large scale structure that are highly clustered.

We do not try to recover these structures because they can not be prominent enough. Since our analysis is bidimensional, we can only detect and use confidently the most prominent structures. Redshifts are needed for a more detailed analysis of cluster substructures.

We list the 55 clusters with significant structures in Table A.1. We give, for each substructure: (1) the name of the parent cluster; (2) the classification of the structure as main (M), subcluster (S), or background (B) together with their order number; (3) right ascension (J2000), and (4) declination (J2000) in decimal degrees of the DEDICA peak; the parameters of the ellipse we obtain from the variance matrix of the coordinates of galaxies in the substructure, i.e. (5) major axis in arcminutes, (6) ellipticity, and (7) position angle in degrees; (8) luminosity (see the next section); (9) χ^2_S.

We make available contour plots of the number density fields of all clusters in Fig. 6 of the electronic version of this Journal. In Fig. 5 we show an example of these plots. Isodensity contours are drawn at ten logarithmic intervals. Galaxies belonging to the systems detected by DEDICA are shown as dots of different colors. We use large symbols for brighter galaxies ($M_V \leq -17.0$) that lie where local densities are higher than the median local density of the structure the galaxy belongs to. We also mark with open symbols the positions of the first- and second-ranked cluster galaxies, BCG1 and BCG2 respectively. Color coding is black, light green, blue, red, magenta, dark green for the main system and the subsequent substructures ordered as in Table A.1.

We describe and analyze in detail our catalog in the next section.

7. Properties of substructures

The first problem we face in order to study the statistical and physical properties of substructures is to determine their association with the main structure. In fact, the main structure itself has to be identified among the structures detected by DEDICA in each frame.

In most cases it is easy to identify the main structure of a cluster since it is located at the center of the frame and it has a high χ^2_S. In two cases (A0168 and A1736) the choice of the main structure is complicated because there are several similar structures near the center of the frame. In these cases we select the main structure for its highest χ^2_S.

At this point we limit our analysis to members of the structure that a) have an absolute magnitude $M_V \leq -17$ (corrected for Galactic absorption) and that b) are in the upper half of the distribution of DEDICA-defined local galaxy densities of the system they belong to. The galaxy density threshold we apply allows us to separate adjacent structures whose definition becomes more uncertain at lower galaxy density levels. The magnitude cut increases the relative weight of the galaxies we use to evaluate the nature of structures in the CMD.

After having identified the main structure, we need to determine which structures in the field of view of a given cluster have to be considered background structures. We consider a structure a physical substructure (or subcluster) if its color-magnitude relation (CMR hereafter) is identical, within the errors, to the CMR of the main structure.

As a first step we define the color-magnitude relation (CMR) of the "whole cluster", i.e. of galaxies in the main structure together with all other galaxies not assigned to any structure by DEDICA. We compute the $(B-V)$ CMR of the Coma cluster from published data (Adami et al. 2006). Then we keep fixed the slope of the linear CMR of Coma and shift it to the mean redshift of the cluster.

In order to determine that the main structure and a substructure are at the same redshift, we evaluate the fraction of background (red) galaxies, f_{bg}, that each structure has in the CMD. If these fractions are identical within the errors (Gehrels 1986), we consider the two structures to be at the same redshift.

In practice we determine f_{bg} by assigning to the background those galaxies of a structure that are redder than a line parallel to the CMR and vertically shifted (i.e. redwards) by 2.33 times the root-mean square of the colors of galaxies in the CMR. We note that the probability that a random variable is greater than 2.33 in a Gaussian distribution is only 1%.

The result of the selection of main structures and substructures is the following: 40 clusters have a total of 69 substructures at the same redshift as the main structure, only 15 clusters are left without substructures. A total of 35 systems are found in the background. Considering a) the number density of poor-to-rich clusters (Mazure et al. 1996; Zabludoff et al. 1993), b) the average luminosity function of clusters (Yagi et al. 2002;

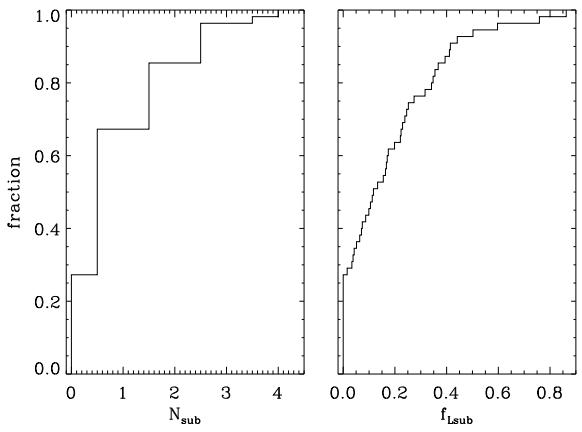

Fig. 7. Cumulative distributions of the two different indicators of subclustering: left panel N_{sub}, right panel f_{Lsub}.

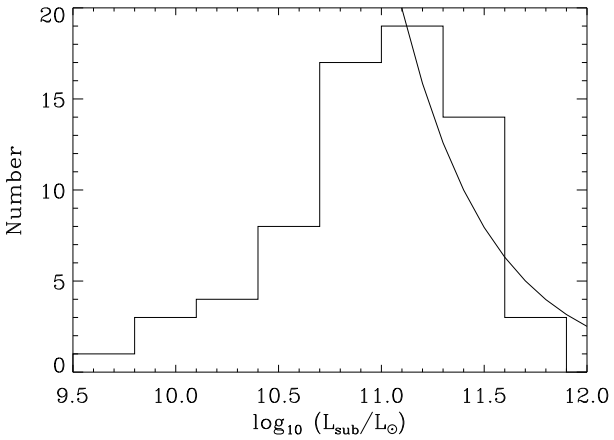

Fig. 8. Observed differential distribution of subcluster luminosities (histogram) and theoretical model (arbitrary scaling; De Lucia et al. 2004).

De Propris et al. 2003), c) the total area covered by the 55 cluster fields, and d) the limiting apparent magnitude corresponding to our absolute magnitude threshold $M_V = -16.0$, we expect to find $\sim 0.5 \pm 0.2$ background systems per cluster field, 28 ± 11 in total. This estimate is consistent with the 35 background systems we find.

The fraction of clusters with subclusters (73%) is higher than generally found in previous investigations (typically $\sim$ 30%, see, e.g., Girardi & Biviano 2002; Flin & Krywult 2006; Lopes et al. 2006, and references therein). Even if we count all undetected clusters as clusters without substructures, this fraction only decreases to 52% (40/77). It is however acknowledged that the fraction of substructured clusters depends, among other factors, on the algorithm used to detect substructures, on the quality and depth of the galaxy catalog. For example Kolokotronis et al. (2001) using optical and X-ray data find that the fraction of clusters with substructures is $\geq$ 45%, Burgett et al. (2004) using a battery of tests detect substructures in 84% of the 25 clusters of their sample.

Having established the "global" fraction of substructured clusters, we now investigate the degree of subclustering of individual clusters, i.e. the distribution of the number of substructures N_{sub} we find in our sample.

We find 15 (27%) clusters without substructures; 22 (40%) clusters with $N_{sub} = 1$; 10 (18%) clusters with $N_{sub} = 2$; 6 (11%) clusters with $N_{sub} = 3$; and 2 (3%) clusters with $N_{sub} = 4$. We plot in the left panel of Fig. 7 the integral distribution of N_{sub}.

The distribution of the level of subclustering does not change when we measure it as the fractional luminosity of subclusters, f_{Lsub}, relative to the luminosity of the whole cluster (see Fig. 7, right panel). The luminosities we estimate are background corrected using the counts of Berta et al. (2006). We use the ellipses output from DEDICA (see previous section) as a measure of the area of subclusters.

We find that N_{sub} and f_{Lsub} are clearly correlated according to the Spearman rank-correlation test.

We now consider the distribution of subcluster luminosities and plot the corresponding histogram in Fig. 8. In the same figure we also plot with arbitrary scaling the power-law $\propto L^{-1}$. This relation is the prediction for the differential mass function of substructures in the cosmological simulations of De Lucia et al. (2004).

Our observations are consistent to within the uncertainties with the theoretical prediction of De Lucia et al. (2004) down to $L \sim 10^{11.2} L_{\odot}$. The disagreement at lower luminosity is expected since: a) below this limit galaxy-sized halos become important among the simulated substructures, and b) only above this limit we expect our catalog to be complete. In fact only subclusters with luminosities brighter than $L = 10^{11.2} L_{\odot}$ have always richnesses that are $\geq 1/3$ of the main structure. This richness limit approximately corresponds to the completeness limit of DEDICA detections according to our simulations (see Sect. 4).

8. Brightest Cluster Galaxies

Here we investigate the relation between BCGs and cluster structures.

We find that, on average, BCG1s are located close to the density peak of the main structures. In projection on the sky, the biweight average (see Beers et al. 1990) distance of BCG1s from the peak of the main system is 72 ± 11 kpc. If we only consider the 44 BCG1s that are on the CMR and are assigned to main systems by DEDICA, the average distance decreases to 56 ± 8 kpc. The fact that BCG1s are close to the center of the system is consistent with current theoretical view on the formation of BCGs (e.g. Dubinski 1998; Nipoti et al. 2004).

BCG2s are more distant than BCG1s from the peak of the main system: the biweight average distance is 345 ± 47 kpc. If we only consider the 26 BCG2s that are on the CMR and are assigned to main systems by DEDICA, the average distance decreases to 161 ± 34 kpc.

Projected distances of BCG2s from density peaks remain larger than those of BCG1s even when we consider the density peak of the structure or substructure they belong to. In Fig. 9 we plot the cumulative distributions of the distances of BCG1s (solid line) and BCG2s (dashed line) from the density peak of their systems. The distributions are different at the $>$ 99.99% level according to a Kolmogorov-Smirnov test (KS-test).

Now we turn to luminosities and find that the magnitude difference between BCG1s and BCG2s, ΔM_{12}, is larger in clusters without substructures than in clusters with substructures. In Fig. 10 we plot the cumulative distributions of ΔM_{12} for clusters with (dashed line) and without (solid line) subclusters.

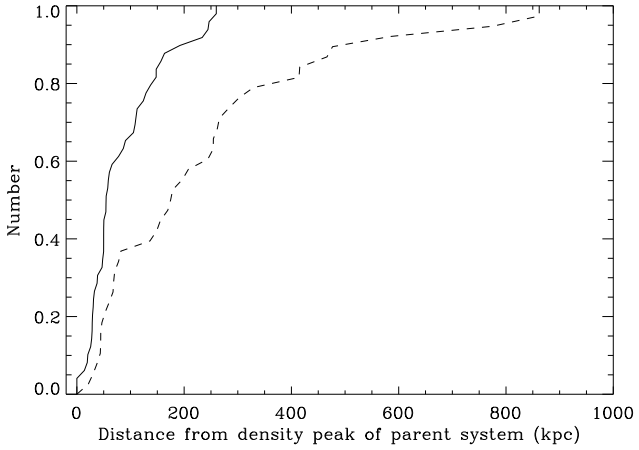

Fig. 9. Cumulative distributions of distances of BCG1 (solid line) and BCG2 (dashed line) from the density peak of their system.

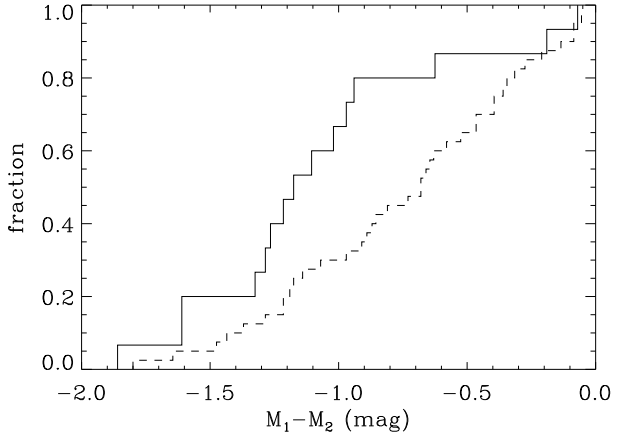

Fig. 10. Cumulative distributions of the magnitude difference between BCG1 and BCG2 in clusters with (dashed line) and without subclusters (solid line).

The two distributions are different according to a KS-test at the 99.1% confidence level. We note that Lin & Mohr (2004) find that ΔM_{12} is independent of cluster properties. These authors however do not consider subclustering.

In order to determine whether the higher values of ΔM_{12} in clusters without subclusters are due to an increased luminosity of the BCG1 (L_1) or to a decreased luminosity of the BCG2 (L_2), we consider the luminosity of the 10^{th} brightest galaxy (L_{10}) as a reference. The biweight average luminosity ratios are $< L_1/L_{10} >= 8.6 \pm 1.0$ and $< L_2/L_{10} >= 3.3 \pm 0.3$ in clusters without substructures, and $< L_1/L_{10} >= 7.1 \pm 0.4$ and $< L_2/L_{10} >= 3.4 \pm 0.2$ in clusters with substructures. We then conclude that the ΔM_{12}-effect is caused by a brightening of the BCG1 relative to the BCG2 in clusters without substructures.

The fact that ΔM_{12} is higher in clusters without substructures can be interpreted, at least qualitatively, in the framework of the hierarchical scenario of structure evolution. Clusters without substructures are likely to be evolved after several merger phases. Their BCG1s have already had time to accrete many galaxies, in particular the more massive ones, which slow down and sink to the cluster center as the result of dynamical friction. Some of these galaxies may even have been BCGs of the merging structures. The simulations by De Lucia & Blaizot (2006) show that the BCG1s continue to increase their mass via cannibalism even at recent times, and that there is a large variance in the mass accretion history of BCG1s from cluster to cluster. The result of such a cannibalism process is an increase of the BCG1 luminosity with respect to other cluster galaxies, and in extreme cases may lead to the formation of fossil groups (Khosroshahi et al. 2006).

However, according to these simulations, only 15% of all BCG1s have accreted > 30% of their mass over the last 2 Gyr, while another 15% have accreted <3% of their mass over the same period. Our results indicate that about 60% of the BCG1s are more than 1 magnitude brighter than the corresponding BCG2s. Given the size and generality of the luminosity differences it would seem that cannibalism alone, even if present along the merging history of a given cluster, cannot account for it. Most of the BCG1s should have then been assembled in early times, as pointed out in the downsizing scenario for galaxy formation (Cowie et al. 1996) and entered that merging history already with luminosity not far form the present one.

9. Summary

In this paper we search for and characterize cluster substructures, or subclusters, in the sample of 77 nearby clusters of the WINGS (Fasano et al. 2006). This sample is an almost complete sample in X-ray flux in the redshift range $0.04 < z < 0.07$.

We detect substructures in the spatial projected distribution of galaxies in the cluster fields using DEDICA (Pisani 1993, 1996) an adaptive-kernel technique. DEDICA has the following advantages for our study of WINGS clusters:

a) DEDICA gives a total description of the clustering pattern, in particular membership probability and significance of structures besides geometrical properties.

b) DEDICA is scale invariant

c) DEDICA does not assume any property of the clusters, i.e. it is completely non-parametric. In particular it does not require particularly rich samples to run effectively.

In order to test DEDICA and to set guidelines for the interpretation of the results of the application of DEDICA to our observations we run DEDICA on several sets of simulated fields containing a cluster with and without subclusters.

We find that: a) DEDICA always identifies both cluster and subcluster even when the substructure richness ratio cluster-to-subcluster is r_{cs}= 8, b) DEDICA recovers a large fraction of members, almost irrespective of the richness of the original structure ($\gtrsim$ 70% in most cases), c) structures with richness ratios $r_{cs} \lesssim 3$ are always distinguishable from noise fluctuations of the poissonian simulated field.

These simulations also allow us to define a threshold that we use to identify significant structures in the observed fields.

We apply our clustering procedure to the 77 clusters of the WINGS sample. We cut galaxy catalogs to the absolute magnitude threshold $M_V = -16.0$ in order to maximize the signal-to-noise ratio of the detected subclusters.

We detect at least one significant structure in 55 (71%) cluster fields. We find that 12 clusters (16%) have no structure above the threshold (undetected). In the remaining 10 (13%) clusters we find significant structures only at the border of the field of view. In absence of a detection in the center of the frame, we consider these border structures unrelated to the target cluster. We also verify that in the CMD these border structures are redder

than expected given the redshift of the target cluster. We consider also these clusters undetected.

We provide the coordinates of all substructures in the 55 clusters together with their main properties.

Using the CMR of the early-type cluster galaxies we separate "true" subclusters from unrelated background structures. We find that 40 clusters out of 55 (73%) have a total of 69 substructures with 15 clusters left without substructures.

The fraction of clusters with subclusters (73%) we identify is higher than most previously published values (typically $\sim 30\%$, see, e.g., Girardi & Biviano 2002, and references therein). It is however acknowledged that the fraction of substructured clusters depends, among other factors, on the algorithm used to detect substructures, on the quality and depth of the galaxy catalog (Kolokotronis et al. 2001; Burgett et al. 2004).

Another important result of our analysis is the distribution of subcluster luminosities. In the luminosity range where our substructure detection is complete ($L \geq 10^{11.2}\, L_{\odot}$), we find that the distribution of subcluster luminosities is in agreement with the power-law $\propto L^{-1}$ predicted for the differential mass function of substructures in the cosmological simulations of De Lucia et al. (2004).

Finally, we investigate the relation between BCGs and cluster structures.

We find that, on average, BCG1s are located close to the density peak of the main structures. In projection on the sky, the biweight average distance of BCG1s from the peak of the main system is 72 ± 11 kpc. BCG2s are significantly more distant than BCG1s from the peak of the main system (345 ± 47 kpc).

The fact that BCG1s are close to the center of the system is consistent with current theoretical view on the formation of BCGs (Dubinski 1998).

A more surprising result is that the magnitude difference between BCG1s and BCG2s, ΔM_{12}, is significantly larger in clusters without substructures than in clusters with substructures. This fact may be interpreted in the framework of the hierarchical scenario of structure evolution (e.g. De Lucia & Blaizot 2006).

References

Abdelsalam H.M., Saha P., Williams L.L.R., Oct. 1998, AJ, 116, 1541
Abell G.O., Neyman J., Scott E.L., 1964, AJ, 69, 529
Abraham R.G., Smecker-Hane T.A., Hutchings J.B., et al., Nov. 1996, ApJ, 471, 694
Adami C., Mazure A., Biviano A., Katgert P., Rhee G., Mar. 1998a, A&A, 331, 493
Adami C., Mazure A., Katgert P., Biviano A., Aug. 1998b, A&A, 336, 63
Adami C., Biviano A., Durret F., Mazure A., Nov. 2005, A&A, 443, 17
Adami C., Picat J.P., Savine C., et al., Jun. 2006, A&A, 451, 1159
Arnaud M., Maurogordato S., Slezak E., Rho J., Mar. 2000, A&A, 355, 461
Arnouts S., de Lapparent V., Mathez G., et al., Jul. 1997, A&AS, 124, 163
Bardelli S., Pisani A., Ramella M., Zucca E., Zamorani G., Oct. 1998a, MNRAS, 300, 589
Bardelli S., Zucca E., Zamorani G., Vettolani G., Scaramella R., May 1998b, MNRAS, 296, 599
Bardelli S., Zucca E., Baldi A., Jan. 2001, MNRAS, 320, 387
Barrena R., Biviano A., Ramella M., Falco E.E., Seitz S., May 2002, A&A, 386, 816
Beers T.C., Flynn K., Gebhardt K., Jul. 1990, AJ, 100, 32
Beers T.C., Gebhardt K., Forman W., Huchra J.P., Jones C., Nov. 1991, AJ, 102, 1581
Bekki K., Jan. 1999, ApJ, 510, L15
Berta S., Rubele S., Franceschini A., et al., Jun. 2006, A&A, 451, 881
Binggeli B., Mar. 1982, A&A, 107, 338
Bird C.M., Jun. 1995, ApJ, 445, L81
Biviano A., Durret F., Gerbal D., et al., Jul. 1996, A&A, 311, 95
Biviano A., Katgert P., Mazure A., et al., May 1997, A&A, 321, 84
Biviano A., Murante G., Borgani S., et al., Sep. 2006, A&A, 456, 23
Böhringer H., Schuecker P., Jun. 2002, Observational signatures and statistics of galaxy Cluster Mergers: Results from X-ray observations with ROSAT, ASCA, and XMM-Newton, 133–162, ASSL Vol. 272: Merging Processes in Galaxy Clusters
Briel U.G., Henry J.P., Boehringer H., Jun. 1992, A&A, 259, L31
Buote D.A., Jun. 2002, X-Ray Observations of Cluster Mergers: Cluster Morphologies and Their Implications, 79–107, ASSL Vol. 272: Merging Processes in Galaxy Clusters
Buote D.A., Xu G., Jan. 1997, MNRAS, 284, 439
Burgett W.S., Vick M.M., Davis D.S., et al., Aug. 2004, MNRAS, 352, 605
Caldwell N., Rose J.A., Feb. 1997, AJ, 113, 492
Caldwell N., Rose J.A., Sharples R.M., Ellis R.S., Bower R.G., Aug. 1993, AJ, 106, 473
Cen R., Aug. 1997, ApJ, 485, 39
Clowe D., Bradač M., Gonzalez A.H., et al., Sep. 2006, ApJ, 648, L109
Cowie L.L., Songaila A., Hu E.M., Cohen J.G., Sep. 1996, AJ, 112, 839
Crone M.M., Evrard A.E., Richstone D.O., Aug. 1996, ApJ, 467, 489
De Lucia G., Blaizot J., Jun. 2006, ArXiv Astrophysics e-prints
De Lucia G., Kauffmann G., Springel V., et al., Feb. 2004, MNRAS, 348, 333
De Propris R., Colless M., Driver S.P., et al., Jul. 2003, MNRAS, 342, 725
de Vaucouleurs G., May 1961, ApJS, 6, 213
Demarco R., Rosati P., Lidman C., et al., Mar. 2005, A&A, 432, 381
Dressler A., Shectman S.A., Apr. 1988, AJ, 95, 985
Dubinski J., Jul. 1998, ApJ, 502, 141
Dubinski J., Aug. 1999, In: Merritt D.R., Valluri M., Sellwood J.A. (eds.) ASP Conf. Ser. 182: Galaxy Dynamics - A Rutgers Symposium, 491–+
Durret F., Forman W., Gerbal D., Jones C., Vikhlinin A., Jul. 1998, A&A, 335, 41
Escalera E., Slezak E., Mazure A., Oct. 1992, A&A, 264, 379
Escalera E., Biviano A., Girardi M., et al., Mar. 1994, ApJ, 423, 539
Ettori S., Fabian A.C., White D.A., Nov. 1998, MNRAS, 300, 837
Fadda D., Slezak E., Bijaoui A., Jan. 1998, A&AS, 127, 335
Fasano G., Marmo C., Varela J., et al., Jan. 2006, A&A, 445, 805
Ferrari C., Maurogordato S., Cappi A., Benoist C., Mar. 2003, A&A, 399, 813
Ferrari C., Arnaud M., Ettori S., Maurogordato S., Rho J., Feb. 2006, A&A, 446, 417
Fitchett M., Merritt D., Dec. 1988, ApJ, 335, 18
Fitchett M.J., 1988, In: Dickey J.M. (ed.) ASP Conf. Ser. 5: The Minnesota lectures on Clusters of Galaxies and Large-Scale Structure, 143–174
Flin P., Krywult J., Apr. 2006, A&A, 450, 9
Gehrels N., Apr. 1986, ApJ, 303, 336
Geller M.J., Beers T.C., Jun. 1982, PASP, 94, 421
Giacintucci S., Venturi T., Bardelli S., et al., Apr. 2006, New Astronomy, 11, 437
Gioia I.M., Henry J.P., Mullis C.R., Ebeling H., Wolter A., Jun. 1999, AJ, 117, 2608
Girardi M., Biviano A., Jun. 2002, Optical Analysis of Cluster Mergers, 39–77, ASSL Vol. 272: Merging Processes in Galaxy Clusters
Girardi M., Fadda D., Giuricin G., et al., Jan. 1996, ApJ, 457, 61
Girardi M., Escalera E., Fadda D., et al., Jun. 1997, ApJ, 482, 41
Gnedin O.Y., Oct. 1999, Ph.D. Thesis
Haines C.P., Clowes R.G., Campusano L.E., Adamson A.J., May 2001, MNRAS, 323, 688
Huo Z.Y., Xue S.J., Xu H., Squires G., Rosati P., Mar. 2004, AJ, 127, 1263
Jeltema T.E., Canizares C.R., Bautz M.W., Buote D.A., May 2005, ApJ, 624, 606
Jones C., Forman W., Jan. 1999, ApJ, 511, 65
Khosroshahi H.G., Ponman T.J., Jones L.R., Oct. 2006, MNRAS, 372, L68
King I., Oct. 1962, AJ, 67, 471
Knebe A., Müller V., Feb. 2000, A&A, 354, 761
Kolokotronis V., Basilakos S., Plionis M., Georgantopoulos I., Jan. 2001, MNRAS, 320, 49
Kriessler J.R., Beers T.C., Jan. 1997, AJ, 113, 80
Lin Y.T., Mohr J.J., Dec. 2004, ApJ, 617, 879
Lopes P.A.A., de Carvalho R.R., Capelato H.V., et al., Sep. 2006, ApJ, 648, 209
Markevitch M., Vikhlinin A., Dec. 2001, ApJ, 563, 95
Markevitch M., Gonzalez A.H., Clowe D., et al., May 2004, ApJ, 606, 819
Materne J., Apr. 1979, A&A, 74, 235
Maughan B.J., Jones L.R., Ebeling H., et al., Apr. 2003, ApJ, 587, 589
Maurogordato S., Proust D., Beers T.C., et al., Mar. 2000, A&A, 355, 848
Mazure A., Katgert P., den Hartog R., et al., Jun. 1996, A&A, 310, 31
Miller N.A., Dec. 2005, AJ, 130, 2541
Miller N.A., Owen F.N., Hill J.M., et al., Oct. 2004, ApJ, 613, 841
Mohr J.J., Fabricant D.G., Geller M.J., Aug. 1993, ApJ, 413, 492
Mohr J.J., Evrard A.E., Fabricant D.G., Geller M.J., Jul. 1995, ApJ, 447, 8
Mohr J.J., Geller M.J., Fabricant D.G., et al., Oct. 1996, ApJ, 470, 724
Moles M., Perea J., del Olmo A., Jan. 1986, MNRAS, 213, 365
Moss C., Whittle M., Sep. 2000, MNRAS, 317, 667
Neumann D.M., Böhringer H., Jul. 1997, MNRAS, 289, 123

Nipoti C., Treu T., Ciotti L., Stiavelli M., Dec. 2004, MNRAS, 355, 1119
Perea J., Moles M., del Olmo A., Jan. 1986a, MNRAS, 219, 511
Perea J., Moles M., del Olmo A., Jan. 1986b, MNRAS, 222, 49
Perea J., del Olmo A., Moles M., Jan. 1990, A&A, 228, 310
Pinkney J., Roettiger K., Burns J.O., Bird C.M., May 1996, ApJS, 104, 1
Pisani A., Dec. 1993, MNRAS, 265, 706
Pisani A., Feb. 1996, MNRAS, 278, 697
Plionis M., Benoist C., Maurogordato S., Ferrari C., Basilakos S., Sep. 2003, ApJ, 594, 144
Poggianti B.M., Bridges T.J., Komiyama Y., et al., Jan. 2004, ApJ, 601, 197
Popesso P., Biviano A., Böhringer H., Romaniello M., Jun. 2006, ArXiv Astrophysics e-prints
Richstone D., Loeb A., Turner E.L., Jul. 1992, ApJ, 393, 477
Roettiger K., Loken C., Burns J.O., Apr. 1997, ApJS, 109, 307
Roettiger K., Stone J.M., Mushotzky R.F., Jan. 1998, ApJ, 493, 62
Rosati P., Tozzi P., Ettori S., et al., Jan. 2004, AJ, 127, 230
Schindler S., Müller E., May 1993, A&A, 272, 137
Schuecker P., Böhringer H., Reiprich T.H., Feretti L., Nov. 2001, A&A, 378, 408
Shane C.D., Wirtanen C.A., Sep. 1954, AJ, 59, 285
Slezak E., Durret F., Gerbal D., Dec. 1994, AJ, 108, 1996
Solanes J.M., Salvador-Solé E., González-Casado G., Mar. 1999, A&A, 343, 733
Thomas P.A., Colberg J.M., Couchman H.M.P., et al., Jun. 1998, MNRAS, 296, 1061
Valdarnini R., Ghizzardi S., Bonometto S., Mar. 1999, New Astronomy, 4, 71
van den Bergh S., 1960, MNRAS, 121, 387
van den Bergh S., Feb. 1961, PASP, 73, 46
van Dokkum P.G., Franx M., Fabricant D., Illingworth G.D., Kelson D.D., Sep. 2000, ApJ, 541, 95
Varela et al., Jan. 2007, A&A, submitted
West M.J., Blakeslee J.P., Nov. 2000, ApJ, 543, L27
West M.J., Oemler A.J., Dekel A., Apr. 1988, ApJ, 327, 1
Xu W., Fang L.Z., Wu X.P., Apr. 2000, ApJ, 532, 728
Yagi M., Kashikawa N., Sekiguchi M., et al., Jan. 2002, AJ, 123, 87
Zabludoff A.I., Geller M.J., Huchra J.P., Ramella M., Oct. 1993, AJ, 106, 1301

Appendix A: The catalog of substructures

We provide here the catalog of substructures. In Table A.1 we give, for each substructure: (1) the name of the parent cluster; (2) the classification of the structure as main (M), subcluster (S), or background (B) together with their order number; (3) right ascension (J2000), and (4) declination (J2000) in decimal degrees of the DEDICA peak; the parameters of the ellipse we obtain from the variance matrix of the coordinates of galaxies in the substructure, i.e. (5) major axis in arcminutes, (6) ellipticity, and (7) position angle in degrees; (8) luminosity; (9) χ^2_S.

ID	class	α_{J2000} (deg)	δ_{J2000} (deg)	a (arcmin)	e	PA (deg)	L ($10^{12}\,L_\odot$)	χ^2_S
A0085	M	10.4752	-9.3025	2.0	0.23	-17.	0.41536	48.4
A0085	S1	10.4410	-9.4430	1.8	0.35	-39.	0.17649	42.9
A0085	S2	10.3947	-9.3501	2.3	0.40	-72.	0.12337	32.8
A0119	M	14.0625	-1.2630	4.1	0.44	-65.	0.83955	63.4
A0119	S1	14.1183	-1.2106	4.6	0.60	-23.	0.26847	50.8
A0119	S2	14.0267	-1.0441	3.4	0.34	80.	0.03592	32.0
A0119	B1	13.9402	-1.4979	3.1	0.39	46.	–	23.5
A0147	M	17.0648	2.2033	3.9	0.45	79.	0.31392	45.2
A0147	S1	16.8673	2.1393	4.1	0.25	-50.	0.05638	24.8
A0147	S2	17.1925	1.9284	4.4	0.38	55.	0.05052	21.4
A0147	B1	17.0753	2.3174	4.4	0.37	75.	–	58.0
A0151	M	17.2186	-15.4219	1.7	0.26	-16.	0.47344	39.9
A0151	S1	17.3516	-15.3652	2.1	0.37	-58.	0.13761	42.9
A0151	S2	17.2632	-15.5564	1.6	0.26	-53.	0.19762	40.9
A0151	B1	17.1375	-15.6116	1.5	0.08	-4.	–	59.0
A0160	M	18.2344	15.5126	3.6	0.37	82.	0.55525	66.7
A0160	S1	18.2483	15.3138	5.0	0.41	85.	0.03120	38.1
A0160	S2	18.1141	15.7501	3.0	0.16	86.	0.15196	28.3
A0160	S3	17.9981	15.4150	3.9	0.41	0.	0.06315	27.8
A0168	M	18.7755	0.3999	3.1	0.32	-11.	0.24492	30.5
A0168	S1	18.8799	0.2993	2.0	0.33	4.	0.06871	28.6
A0193	M	21.2894	8.6994	2.1	0.08	36.	0.61982	105.7
A0193	B1	20.9945	8.6119	4.9	0.45	-1.	–	39.1
A0311	M	32.3793	19.7722	2.3	0.19	43.	0.43320	44.0
A0376	M	41.4276	36.9517	1.7	0.07	-67.	0.13477	40.8
A0376	S1	41.5569	36.9214	4.4	0.49	-22.	0.24350	33.6
A0500	M	69.6476	-22.1308	2.0	0.31	16.	0.41203	45.5
A0500	S1	69.5915	-22.2377	2.3	0.19	36.	0.20520	47.3
A0602	M	118.3638	29.3528	1.8	0.55	-46.	0.20112	55.4
A0602	S1	118.1848	29.4145	2.3	0.52	31.	0.08470	34.8
A0671	M	127.1237	30.4269	1.6	0.24	-51.	0.68582	69.8
A0671	S1	127.2241	30.4342	2.0	0.40	-5.	0.19736	44.3
A0671	S2	127.1617	30.2967	1.9	0.24	-90.	0.13778	43.0
A0754	M	137.1073	-9.6370	2.0	0.25	53.	0.56063	46.8
A0754	S1	137.3707	-9.6760	3.2	0.53	-8.	0.30590	54.9
A0754	S2	137.2619	-9.6367	1.7	0.14	76.	0.23734	51.2
A0957x	M	153.4095	-0.9259	2.0	0.09	-83.	0.42106	38.6
A0957x	B1	153.5517	-0.7023	2.2	0.44	-63.	–	37.9
A0970	M	154.3595	-10.6921	1.5	0.27	-30.	0.46130	62.5
A0970	S1	154.2369	-10.6422	1.7	0.15	15.	0.13660	42.3
A0970	B1	154.1833	-10.6771	1.8	0.23	-76.	–	32.2
A1069	M	159.9418	-8.6883	2.8	0.31	52.	0.37270	50.2
A1069	S1	159.9286	-8.5506	2.4	0.23	88.	0.18532	32.7
A1069	B1	159.7678	-8.9262	3.5	0.55	77.	–	54.7
A1291	M	173.0467	56.0255	2.5	0.51	-11.	0.25272	32.1
A1291	S1	172.9090	56.1872	1.4	0.48	-82.	0.03530	37.6
A1631a	M	193.2410	-15.3413	1.4	0.35	40.	0.20077	33.9
A1736	M	202.0097	-27.3131	3.1	0.35	58.	0.41824	52.1
A1736	S1	201.7305	-27.0170	2.8	0.32	9.	0.24023	42.6
A1736	S2	201.7662	-27.4067	3.4	0.28	7.	0.14528	42.3
A1736	S3	201.5672	-27.4291	2.7	0.44	73.	0.16926	40.4
A1736	S4	201.9057	-27.1600	3.5	0.21	-1.	0.24192	32.9
A1736	S5	201.7036	-27.1236	3.0	0.39	-12.	0.40395	31.7
A1795	M	207.1911	26.5586	0.6	0.17	55.	0.12341	52.4

ID	class	α_{J2000} (deg)	δ_{J2000} (deg)	a (arcmin)	e	PA (deg)	L ($10^{12}\,L_{\odot}$)	χ^2_S
A1795	S1	207.2329	26.7362	1.3	0.38	82.	0.05123	46.7
A1831	M	209.8120	27.9714	1.9	0.43	9.	1.08418	56.0
A1831	S1	209.7356	28.0636	2.1	0.34	41.	0.36295	59.7
A1831	B1	209.5725	28.0206	1.7	0.25	-10.	–	47.7
A1991	M	223.6405	18.6390	2.3	0.54	-78.	0.28195	40.3
A1991	S1	223.7575	18.7812	2.5	0.32	41.	0.11412	49.9
A1991	B1	223.7683	18.7022	1.7	0.31	71.	–	36.6
A2107	M	234.9497	21.8075	2.7	0.19	48.	0.50994	61.1
A2107	B1	235.0699	22.0127	4.3	0.48	83.	–	32.9
A2107	B2	235.1409	21.8276	2.4	0.10	55.	–	20.4
A2124	M	236.2400	36.0990	1.3	0.24	32.	0.41727	43.3
A2124	B1	236.0207	36.1779	1.6	0.22	34.	–	59.7
A2149	M	240.3723	53.9406	1.5	0.46	-10.	0.37347	48.7
A2169	M	243.4867	49.1875	0.6	0.22	72.	0.15358	34.2
A2256	M	255.9260	78.6412	1.9	0.29	-86.	1.46563	95.6
A2256	B1	256.3094	78.4886	2.2	0.48	75.	–	48.2
A2256	B2	256.6024	78.4283	2.0	0.12	-88.	–	46.8
A2399	M	329.3693	-7.7772	3.5	0.64	-26.	0.40505	38.8
A2415	M	331.3829	-5.5444	2.3	0.23	-60.	0.36780	44.8
A2415	S1	331.5610	-5.3960	2.3	0.33	52.	0.05032	33.9
A2415	B1	331.3800	-5.4017	1.9	0.34	32.	–	41.4
A2415	B2	331.3295	-5.3890	1.6	0.41	4.	–	37.3
A2457	M	338.9462	1.4765	4.3	0.50	-84.	0.88720	107.3
A2457	S1	339.0392	1.6459	4.1	0.65	-50.	0.05960	23.1
A2457	B1	339.0667	1.3266	5.6	0.53	77.	–	73.8
A2572a	M	349.3192	18.7197	2.9	0.39	23.	0.44749	47.8
A2572a	S1	349.1122	18.5320	4.1	0.25	8.	0.07320	34.5
A2572a	S2	349.3851	18.5395	2.6	0.31	67.	0.05345	25.1
A2572a	S3	349.0037	18.7220	3.2	0.34	86.	0.00884	20.5
A2593	M	351.0766	14.6539	1.1	0.25	58.	0.28333	33.8
A2593	S1	351.0677	14.4048	2.2	0.42	80.	0.09810	27.0
A2622	M	353.7384	27.3856	3.1	0.09	76.	0.48920	68.1
A2622	S1	353.4880	27.2877	4.2	0.35	46.	0.03070	35.1
A2622	B1	353.7837	27.3182	3.0	0.49	-5.	–	53.7
A2622	B2	353.8009	27.6217	2.6	0.38	68.	–	29.9
A2657	M	356.1725	9.1818	4.5	0.47	22.	0.27061	49.6
A2657	S1	356.2755	9.1799	3.2	0.35	10.	0.20771	34.0
A2657	B1	355.9569	8.9422	2.8	0.06	-10.	–	38.6
A2665	M	357.7050	6.1582	3.6	0.26	71.	0.67950	121.8
A2665	S1	357.4003	5.8659	4.9	0.64	84.	0.01780	17.5
A2665	B1	357.8218	6.3522	3.5	0.44	-50.	–	32.7
A2734	M	2.8363	-28.8652	3.4	0.33	3.	0.48700	56.3
A2734	S1	2.6950	-28.7728	4.0	0.27	-7.	0.18970	55.0
A2734	S2	2.6987	-29.0394	3.2	0.24	55.	0.03030	43.3
A2734	S3	2.5727	-29.0562	3.4	0.51	84.	0.03100	33.1
A2734	B1	2.7701	-28.6488	3.7	0.39	14.	–	28.0
A3128	M	52.4825	-52.5764	2.2	0.17	-36.	0.40452	37.2
A3128	S1	52.7366	-52.7089	4.1	0.44	-9.	0.25240	51.8
A3128	S2	52.6655	-52.4413	2.3	0.32	-65.	0.19646	51.0
A3128	S3	52.3697	-52.7570	3.2	0.47	81.	0.17169	39.0
A3158	M	55.7477	-53.6334	2.6	0.62	2.	0.70205	52.8
A3158	S1	55.8382	-53.6780	3.4	0.58	10.	0.45553	53.4
A3266	M	67.7893	-61.4637	1.1	0.27	-72.	0.42993	63.5
A3376	M	90.1628	-39.9950	2.5	0.14	-43.	0.33708	43.1
A3376	S1	90.4344	-39.9776	2.7	0.20	-4.	0.21279	59.8
A3376	S2	90.4712	-39.7946	2.1	0.39	-88.	0.00904	31.2
A3528b	M	193.5928	-29.0136	1.3	0.04	-24.	0.65638	66.4
A3528b	S1	193.6030	-29.0721	1.3	0.26	10.	0.16706	59.0
A3530	M	193.9098	-30.3606	1.9	0.26	33.	0.53043	34.9
A3532	M	194.3035	-30.3732	3.6	0.52	-44.	0.76920	51.1
A3532	B1	194.0413	-30.2130	3.8	0.38	66.	–	56.3

ID	class	α_{J2000} (deg)	δ_{J2000} (deg)	a (arcmin)	e	PA (deg)	L ($10^{12}\,L_{\odot}$)	χ^2_S
A3558	M	201.9587	-31.4892	4.9	0.54	49.	1.14860	64.1
A3558	B1	202.2501	-31.6887	2.6	0.49	44.	–	37.6
A3562	M	203.4603	-31.6812	2.5	0.18	82.	0.39087	42.4
A3562	S1	203.1622	-31.7742	4.0	0.40	-86.	0.15010	51.1
A3562	S2	203.3137	-31.6953	3.6	0.40	76.	0.11706	41.0
A3562	S3	203.6982	-31.7171	2.5	0.21	-50.	0.07820	36.7
A3562	S4	203.6541	-31.5969	4.0	0.55	-81.	0.06542	30.3
A3667	M	303.1637	-56.8598	2.1	0.14	23.	0.56803	42.0
A3667	S1	303.5297	-56.9660	3.0	0.39	-86.	0.27086	39.2
A3667	S2	302.7241	-56.6674	1.5	0.17	75.	0.28948	34.0
A3667	S3	302.7081	-56.7557	2.3	0.39	12.	0.09961	33.7
A3716	M	312.9910	-52.7677	4.7	0.38	36.	0.76450	77.9
A3716	S1	312.9769	-52.6434	3.5	0.22	-6.	0.49159	56.9
A3716	B1	312.7735	-52.8976	4.1	0.40	28.	–	48.4
A3716	B2	313.1888	-52.4785	3.2	0.23	21.	–	22.6
A3880	M	336.9796	-30.5474	3.8	0.33	-50.	0.25840	44.1
A3880	B1	336.8684	-30.8171	2.5	0.30	64.	–	30.9
A3880	B2	336.7356	-30.7839	2.7	0.35	46.	–	28.4
IIZW108	M	318.4443	2.5706	2.6	0.38	42.	0.49940	33.4
IIZW108	S1	318.6247	2.5533	3.2	0.36	-14.	0.08565	42.3
IIZW108	B1	318.3335	2.7751	1.6	0.24	43.	–	44.5
IIZW108	B2	318.5190	2.8039	2.5	0.44	22.	–	33.6
MKW3s	M	230.3916	7.7281	2.3	0.30	-8.	0.37614	48.7
MKW3s	S1	230.4576	7.8769	3.3	0.46	-22.	0.04585	39.3
MKW3s	B1	230.7349	7.8882	2.0	0.40	16.	–	25.5
RX0058	M	14.5875	26.8816	2.4	0.22	-31.	0.31967	44.2
RX0058	S1	14.7652	27.0424	3.8	0.60	64.	0.31661	50.6
RX0058	B1	14.4012	26.7041	3.3	0.08	-12.	–	28.9
RX1740	M	265.1398	35.6416	2.8	0.21	-26.	0.17896	42.1
RX1740	S1	265.2600	35.4366	3.3	0.22	38.	0.01946	31.7
RX1740	S2	264.8688	35.6053	3.7	0.52	28.	0.01340	27.9
RX1740	S3	265.0744	35.8116	3.5	0.44	-7.	0.01166	21.8
Z2844	M	150.7281	32.6483	2.9	0.20	-85.	0.10143	48.3
Z2844	S1	150.6524	32.7621	5.2	0.58	63.	0.04930	50.5
Z2844	S2	150.5821	32.8890	2.6	0.39	0.	0.00395	23.1
Z8338	M	272.7447	49.9078	3.0	0.37	-67.	0.45876	43.1
Z8338	S1	272.8606	49.7916	3.2	0.11	62.	0.05549	31.9
Z8338	S2	272.6903	49.9737	3.1	0.67	62.	0.07089	25.7
Z8338	B1	272.4479	49.6815	1.7	0.18	9.	–	25.8
Z8852	M	347.6024	7.5824	2.7	0.41	-45.	0.76110	67.9
Z8852	S1	347.5926	7.3999	5.8	0.56	62.	0.12022	32.4
Z8852	S2	347.6986	7.8018	2.3	0.13	81.	0.02493	25.5
Z8852	B1	347.7381	7.6808	2.1	0.25	-73.	–	35.9
Z8852	B2	347.4951	7.8165	2.4	0.21	72.	–	27.0

Online Material

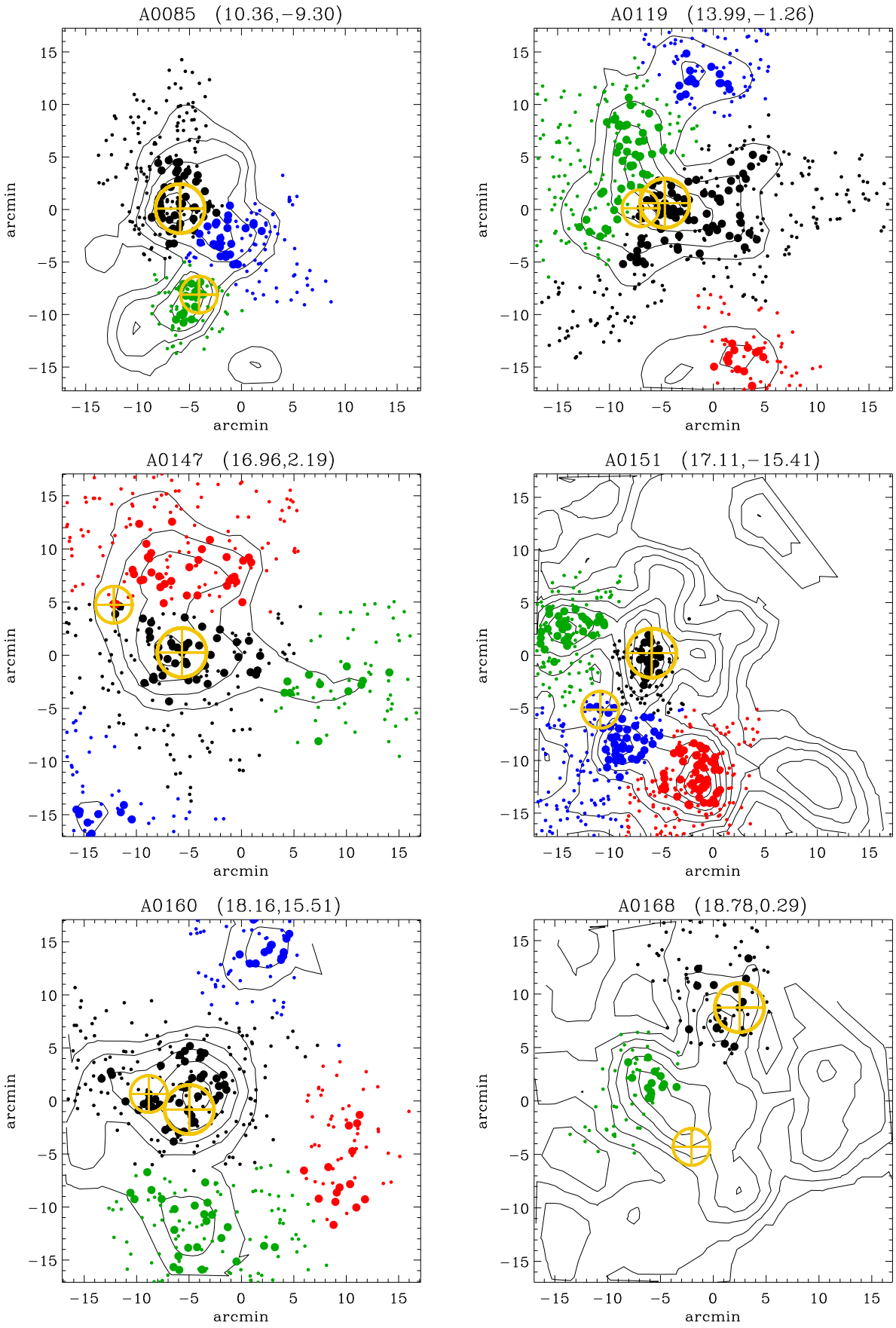

Fig. 6. Isodensity contours (logarithmically spaced) of the 55 clusters with significant structures. The title lists the coordinates of the center. The orientation is East to the left, North to the top. Galaxies belonging to the systems detected by DEDICA are shown as dots of different colors. Black, light green, blue, red, magenta, dark green are for the main system and the subsequent substructures ordered as in Table A.1. Large symbols are for galaxies with $M_V \leq -17.0$ that lie where local densities are higher than the median local density of the structure the galaxy belongs to. Open symbols mark the positions of the first- and second-ranked cluster galaxies, BCG1 and BCG2 respectively.

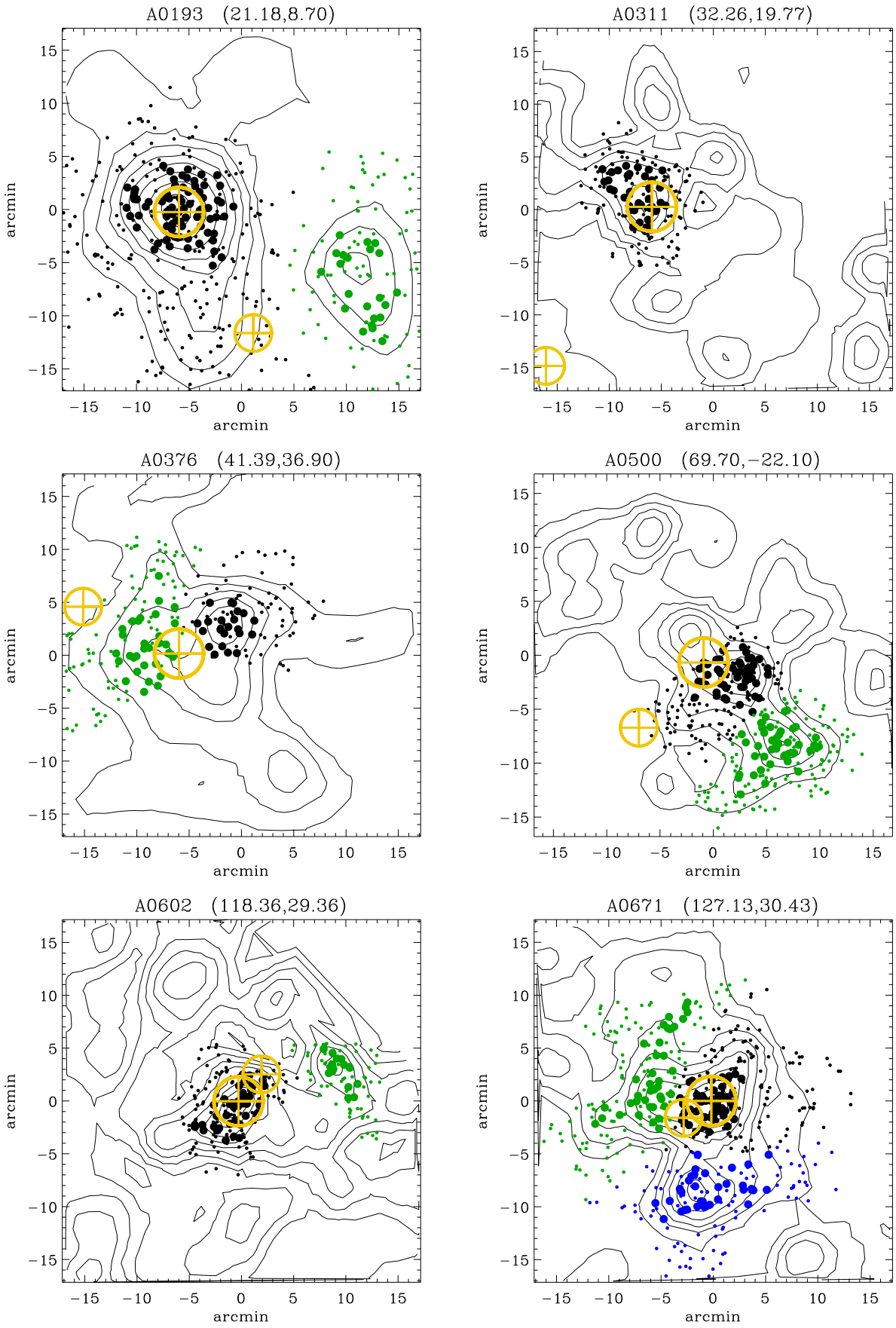

Fig. 6. (continued)

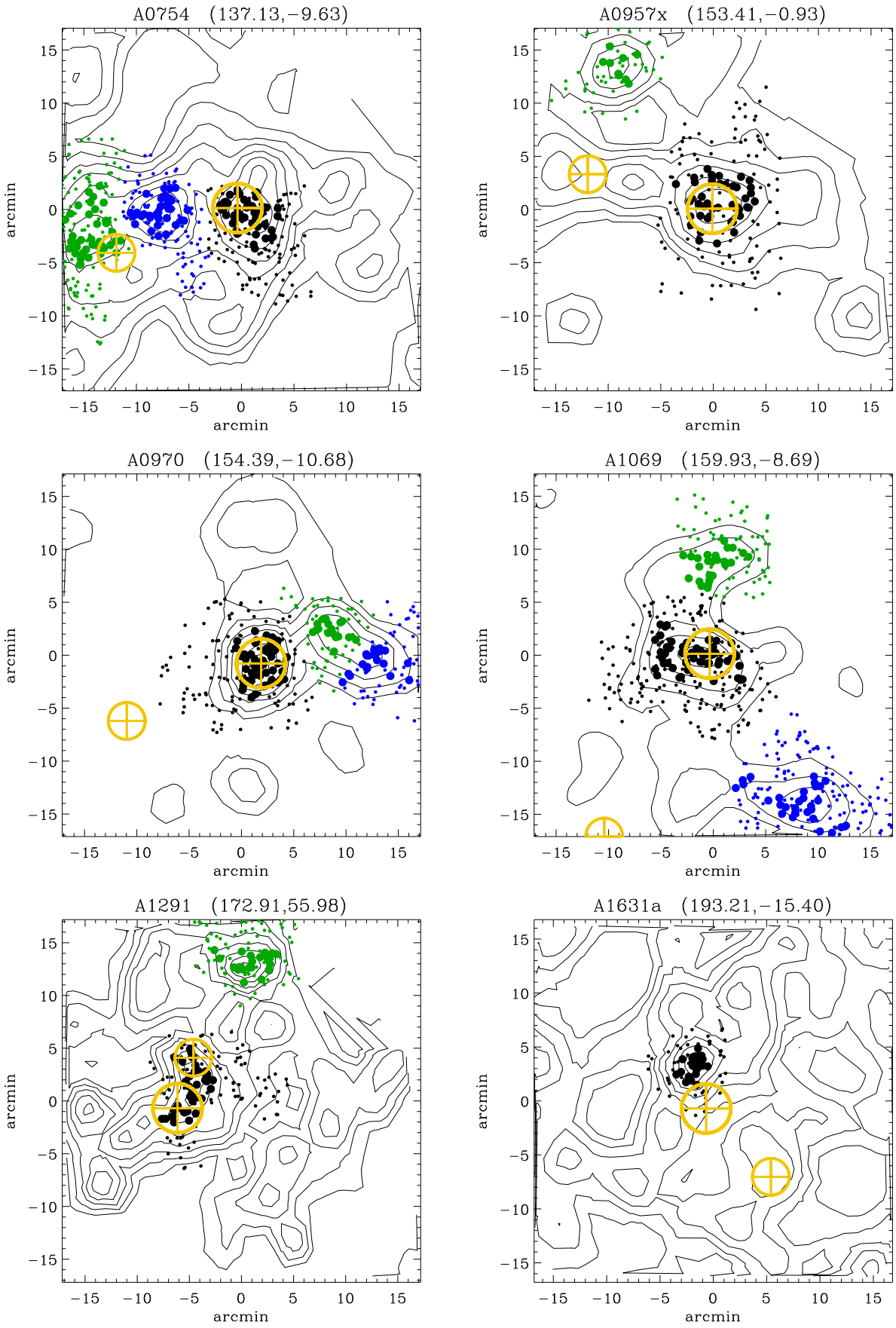

Fig. 6. (continued)

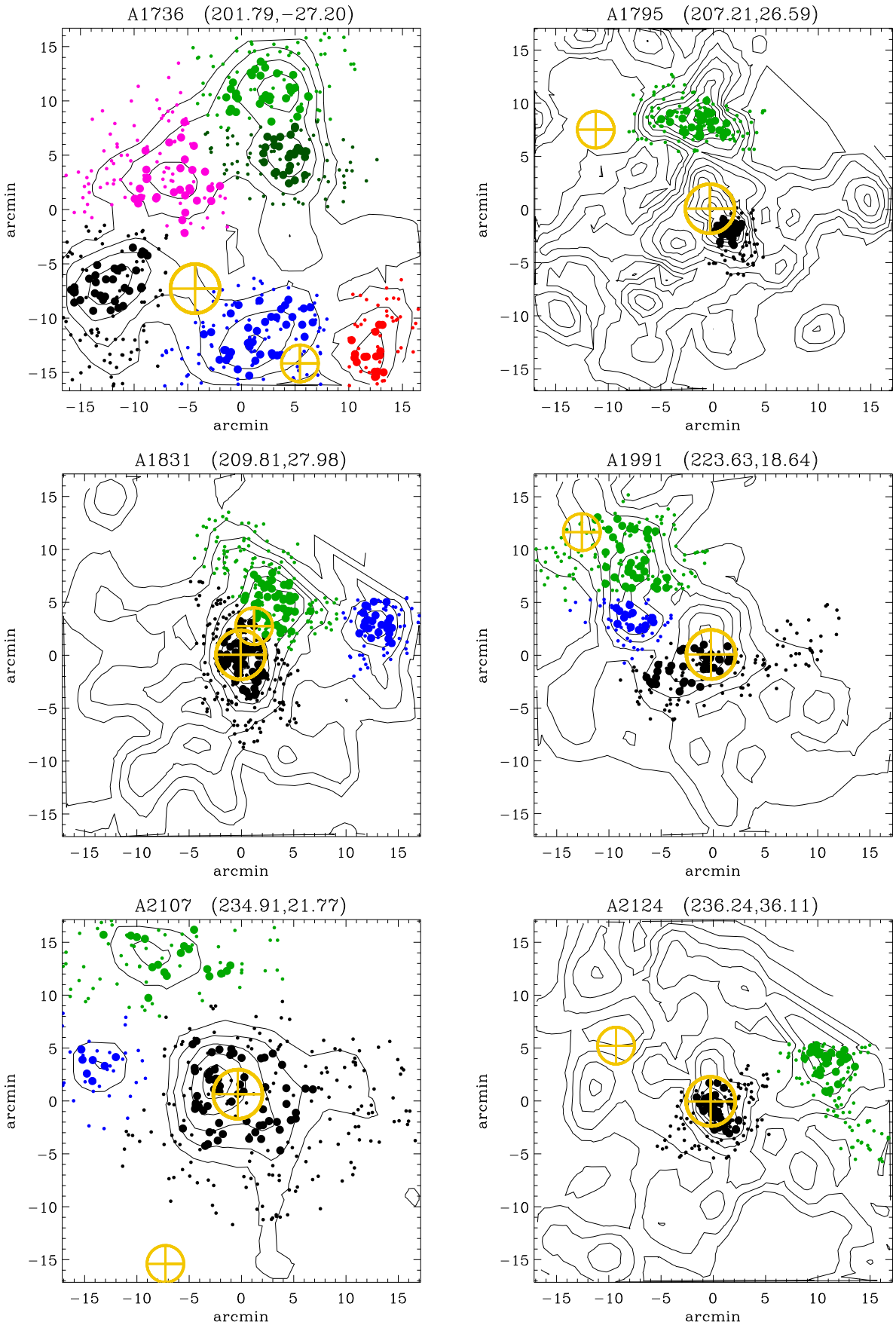

Fig. 6. (continued)

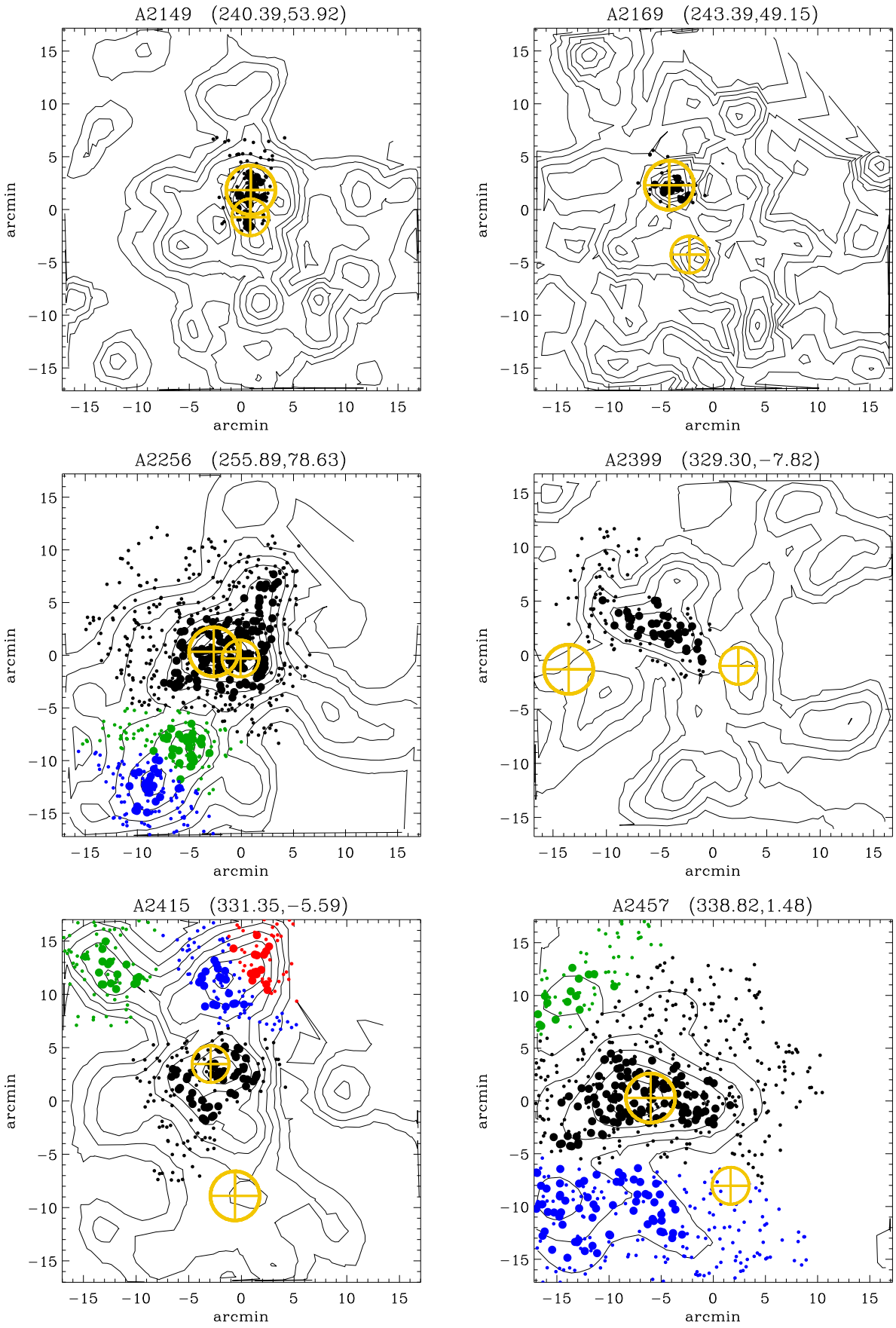

Fig. 6. (continued)

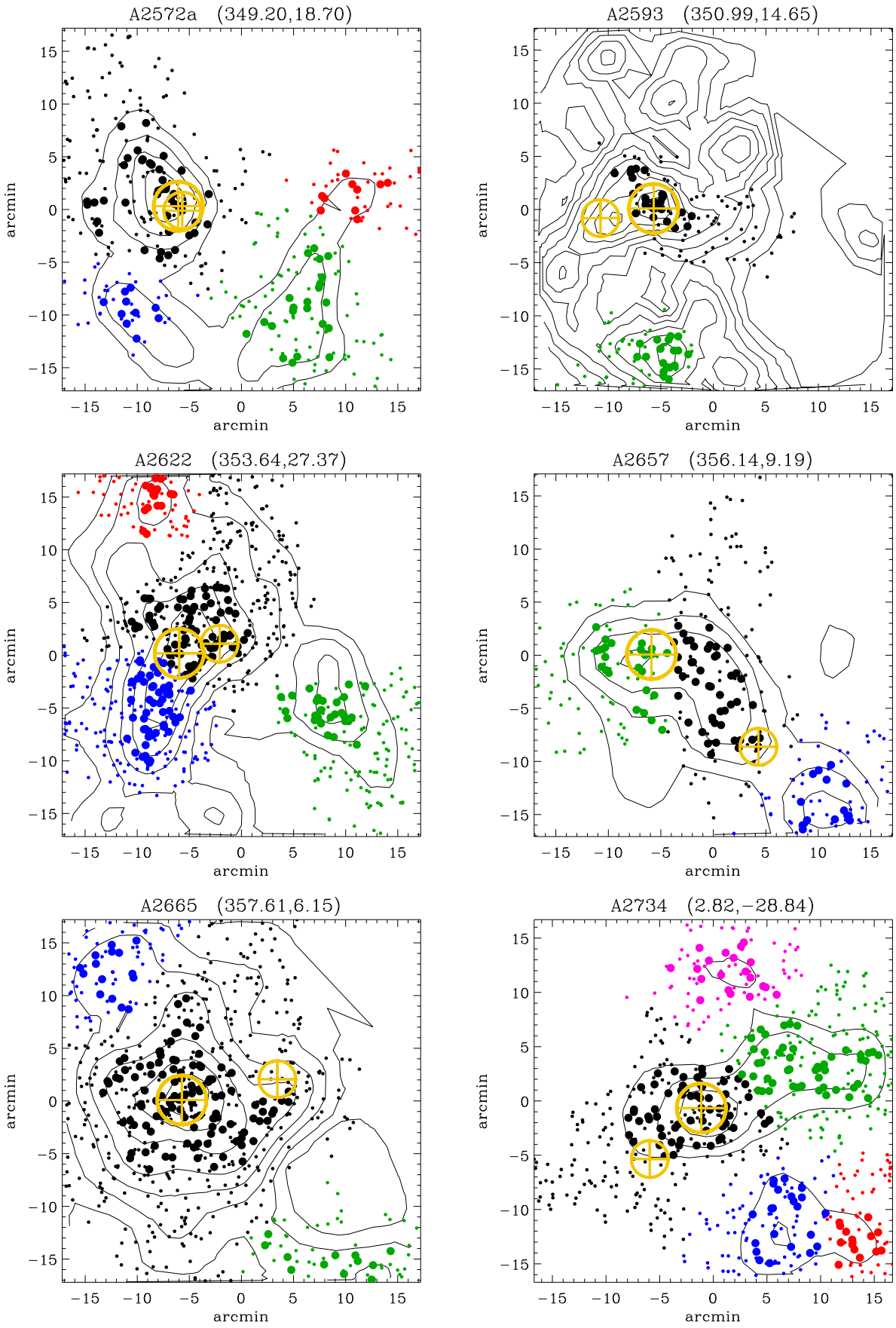

Fig. 6. (continued)

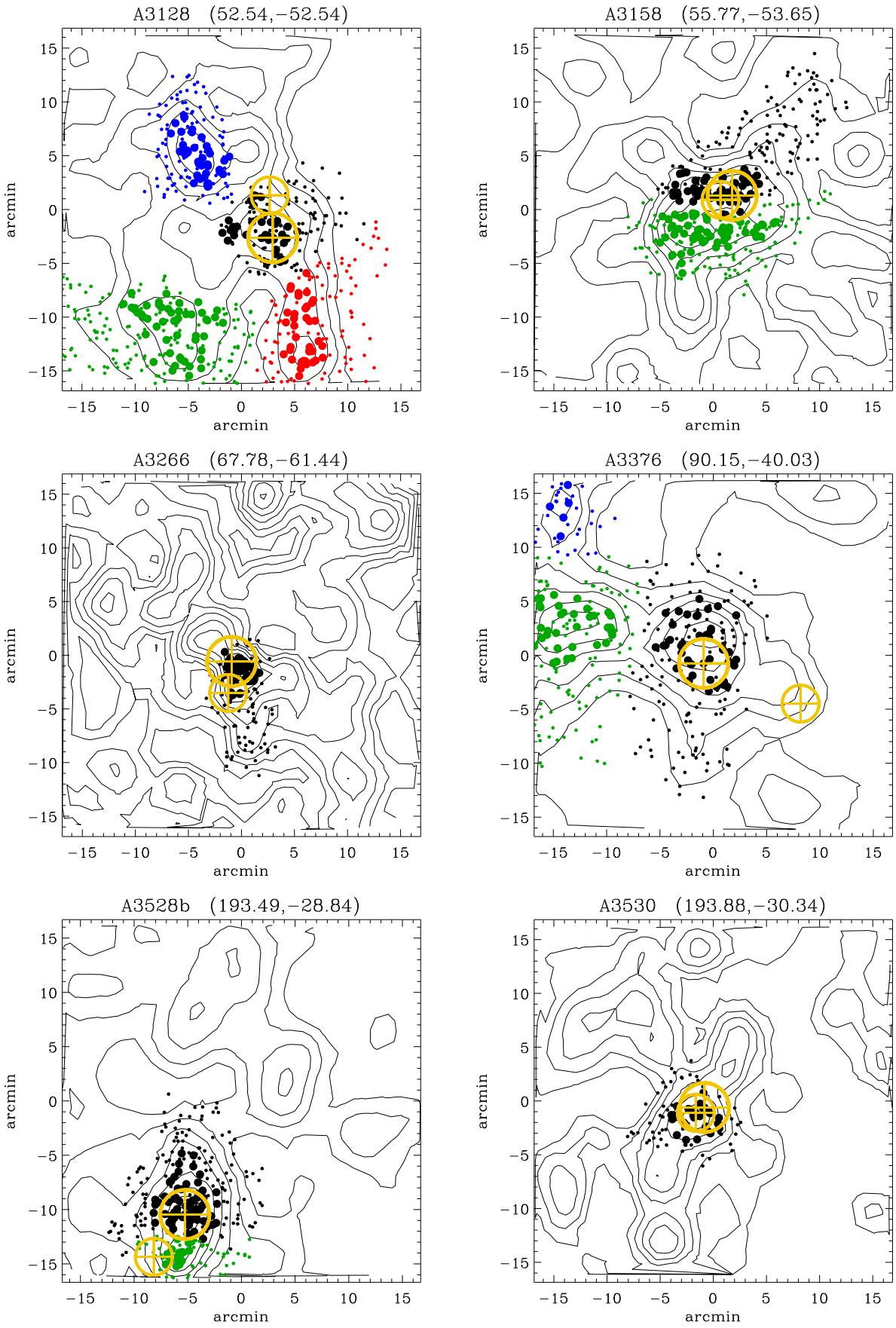

Fig. 6. (continued)

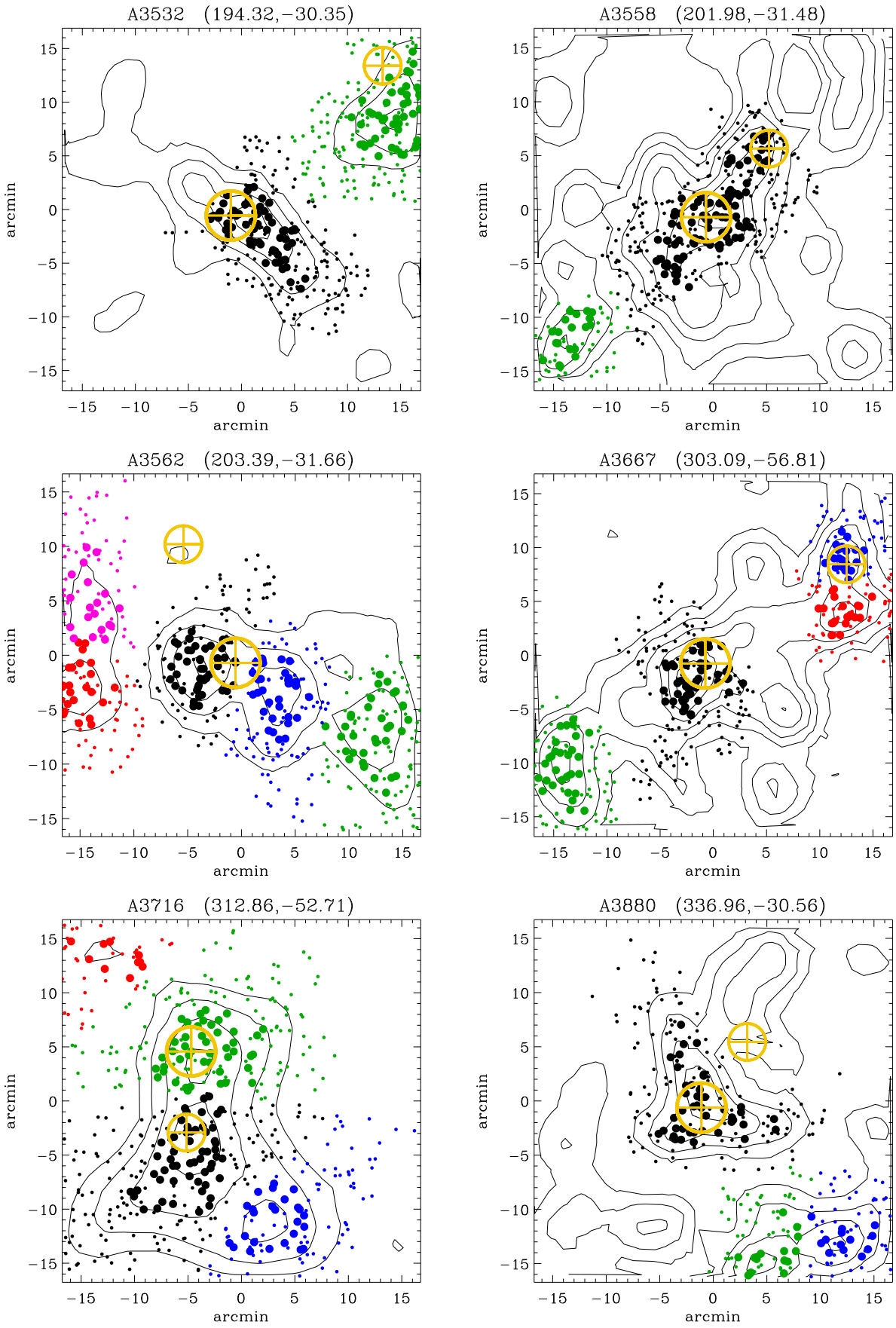

Fig. 6. (continued)

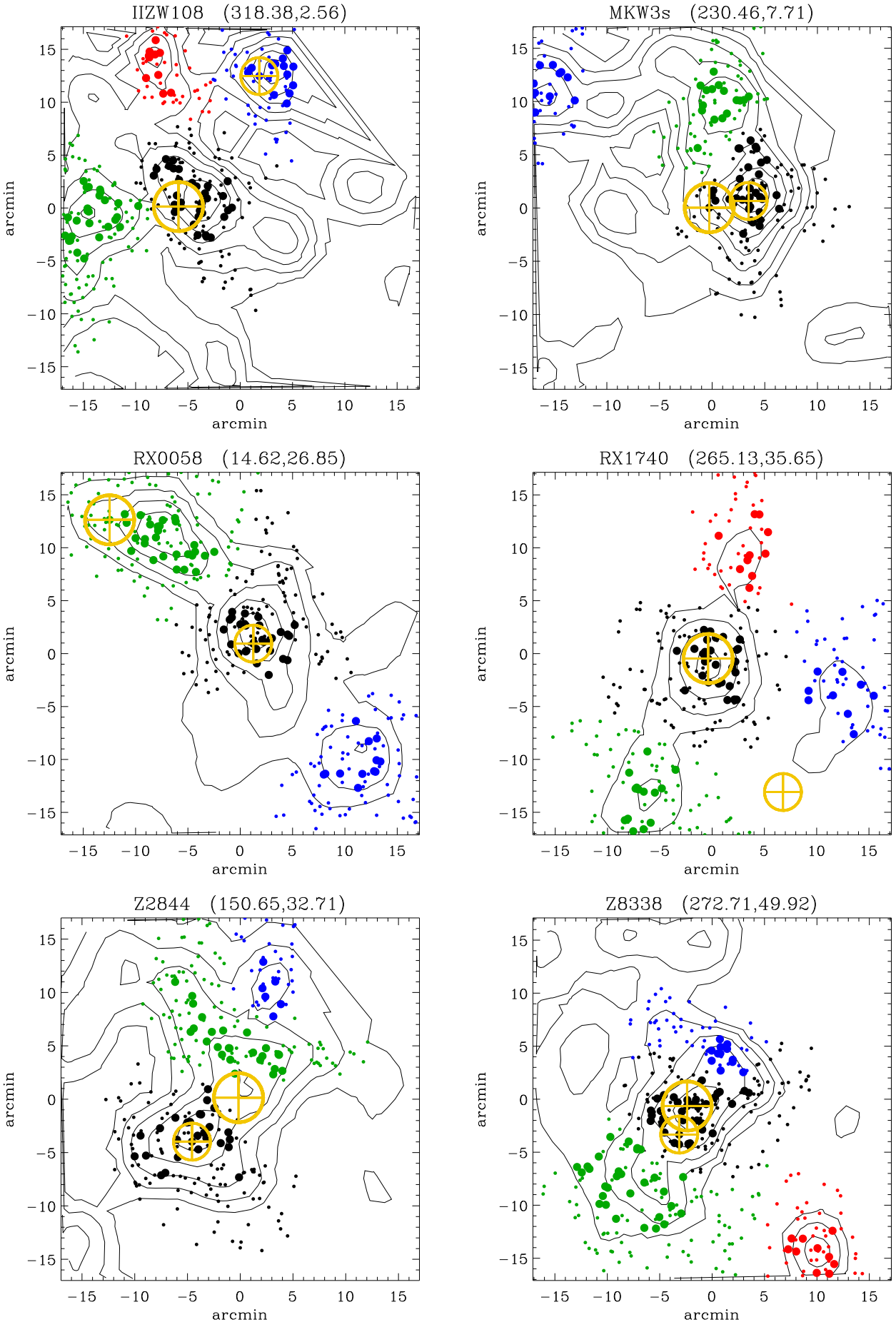

Fig. 6. (continued)

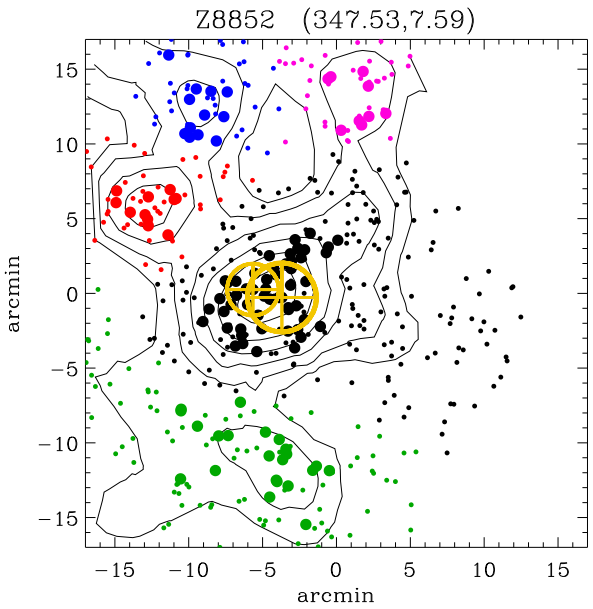

Fig. 6. (continued)